NASA Technical Memorandum 102207

A Two-Dimensional Adaptive-Wall Test Section with Ventilated Walls in the Ames 2- by 2-Foot Transonic Wind Tunnel

Edward T. Schairer, George Lee,
and T. Kevin McDevitt

August 1989

National Aeronautics and
Space Administration

NASA Technical Memorandum 102207

A Two-Dimensional Adaptive-Wall Test Section with Ventilated Walls in the Ames 2- by 2-Foot Transonic Wind Tunnel

Edward T. Schairer and George Lee, Ames Research Center, Moffett Field, California
T. Kevin McDevitt, Complere, Inc., Palo Alto, California

August 1989

National Aeronautics and
Space Administration

Ames Research Center
Moffett Field, California 94035

A TWO-DIMENSIONAL ADAPTIVE-WALL TEST SECTION WITH VENTILATED WALLS IN THE AMES 2- BY 2-FOOT TRANSONIC WIND TUNNEL

Edward T. Schairer, George Lee, and T. Kevin McDevitt[1]

Ames Research Center

SUMMARY

The first tests conducted in the adaptive-wall test section of the Ames Research Center's 2- by 2-Foot Transonic Wind Tunnel are described. A procedure was demonstrated for reducing wall interference in transonic flow past a two-dimensional airfoil by actively controlling flow through the slotted walls of the test section. Flow through the walls was controlled by adjusting pressures in compartments of plenums above and below the test section. Wall interference was assessed by measuring (with a laser velocimeter) velocity distributions along a contour surrounding the model, and then checking those measurements for their compatibility with free-air far-field boundary conditions. Plenum pressures for minimum wall interference were determined from empirical influence coefficients.

An NACA 0012 airfoil was tested at angles of attack of 0° and 2°, and at Mach numbers between 0.70 and 0.85. In all cases the wall-setting procedure greatly reduced wall interference. Wall interference, however, was never completely eliminated, primarily because the effect of plenum pressure changes on the velocities along the contour could not be accurately predicted.

INTRODUCTION

Since the early 1970s, researchers around the world have been developing wind-tunnel test sections that allow flow conditions at the walls to be adjusted to minimize wall interference. The principal reason for this interest has been that traditional methods of "correcting" wind-tunnel data for wall interference are often inadequate, particularly in flows that are represented by nonlinear equations. In addition, the development of simple algorithms for determining the necessary wall adjustments and advances in computer automation have promised to make manageable the problem of controlling the walls.

What distinguishes modern "adaptive-wall" test sections from earlier test sections with adjustable walls (refs. 1-3) is that the wall settings for free-air flow can be determined from flow measurements made at or near the walls without any information about the model. Specifically, the walls are adjusted until flow measurements along a contour surrounding the model (for example, in two dimensions, axial and vertical velocity distributions) are compatible with free-air, far-field boundary conditions. Free-air compatibility is established by solving for the imaginary, infinite flow in the region outside the contour, subject to the measured distribution of one flow quantity along the contour.

---

[1]Present address: Complere, Inc., Palo Alto, California.

Two approaches to controlling flow conditions at the walls have been demonstrated. The first and simplest is to bend impermeable, flexible walls to conform to free-air streamlines. This approach is attractive because the shapes of the walls and the pressure distributions along them—both easily measured—can be used to predict the free-air wall shapes. In addition, the wall shapes can be quickly and directly controlled. There must be some accounting, however, for the effect of the wall boundary layers on the wall shape. This effect becomes especially unpredictable when the shock wave from the model extends to the wall and causes the boundary layer to separate.

Flexible walls are particularly simple in two dimensions, and they have been used in many very successful experiments (refs. 4-8). Two two-dimensional, cryogenic test sections—NASA Langley's 0.3-Meter Wind Tunnel and ONERA's T2 Tunnel—are currently used for "production" testing (refs. 5 and 6).

In three dimensions, however, flexible walls present difficult mechanical problems since the required wall shapes may include double curvatures. The most ambitious attempts to solve these problems have been at Deutsche Forschungs- und Versuchsanstalt für Luft- und Raumfahrt (DFVLR), where a test section with walls formed by a cylindrical rubber tube was developed (ref. 9), and at the Technical University of Berlin, where the potential of octagonal tests sections has been investigated at transonic and supersonic speeds (ref. 8).

The second approach to shaping streamlines in the test section is to control the airflow through rigid, ventilated walls. This can be done either by dividing the plenum surrounding such test sections into compartments and controlling the pressure in each compartment, or by dividing the walls into panels whose porosities can be independently adjusted. The required flow measurements cannot be made at the walls because the flow there is generally complex and turbulent. Thus, the flow-measurement problem is much more difficult in the ventilated wall test section than it is in a flexible-wall test section. In addition, there is no direct relationship between the wall controls and the measured flow conditions along the contour. On the other hand, since the contour is displaced from the walls, there is no boundary layer to contend with in evaluating the outer-flow solution. Another advantage of the ventilated-wall approach is that the plenum compartments or wall panels can be arranged to provide the cross-stream wall control needed for three-dimensional testing. Several two- and three-dimensional ventilated, adaptive-wall experiments have been reported (refs. 10-16).

At Ames Research Center, the original, long-term goal of adaptive-wall research was to develop technology that could be applied in production, three-dimensional transonic wind tunnels. We chose to develop test sections with rigid ventilated walls because this approach seemed more promising than flexible walls for three-dimensional testing. And we investigated test sections with slotted walls and segmented plenums rather than variable-porosity walls because most of the transonic wind tunnels at Ames have slotted walls and because the slats between the slots provide space for windows.

Two-dimensional pilot tests were conducted in a small, in-draft wind tunnel (ref. 12). These tests demonstrated the key elements that were later incorporated into the design of the 2- by 2-ft test section. In particular, flow measurements were made through transparent sidewalls by a one-component laser velocimeter; empirical influence-coefficients were used to relate the flow measurements to pressures in the plenum compartments; and a dedicated minicomputer performed on-line, linear interference calculations. The only aspect of the tests that was not automated was the adjustment of valves that controlled

pressures in the plenum compartments. These valves were adjusted manually according to the computer's instructions.

The success of the pilot tests encouraged us to design a two-dimensional test section for the 2- by 2-ft wind tunnel that would be suitable for production testing. Improvements over the pilot test section were to include more plenum compartments (32 per wall instead of 10); automatic wall control; the capability to measure two components of velocity rather than just one; and outer-flow solutions that account for nonlinear effects. In addition, a new control system was required for existing pumps that would supply high- and low-pressure air to the test section.

The first tests in the new test section were completed in October 1988. An NACA 0012 airfoil was tested at atmospheric pressure, at angles of attack of 0° and 2°, and at Mach numbers between 0.70 and 0.85. The purpose of the test was to verify the operation of the test section and its systems and to demonstrate an automatic wall-adjustment procedure. Because little time was allocated for the tests, no attempt was made to optimize the procedure, which would be necessary for production testing. This paper describes the test section and instrumentation, the calibration of the test section, and the results of the first adaptive-wall tests.

SYMBOLS

c	model chord length
C_n	normal force coefficient
C_p	pressure coefficient
M	free-stream Mach number
p	pressure
p_t	total pressure
R	Reynolds number
u	axial perturbation velocity
U	free-stream velocity
w	vertical velocity
x,ξ	axial distance from model leading edge, positive downstream
z,η	distance above test-section centerline

α angle of attack, stream angle, deg

β $\sqrt{1-M^2}$

Subscripts:

m model-induced (free air)

p in pressure manifold

v in vacuum reservoir

w wall-induced

∞ free stream

EQUIPMENT

The test-section area and control room of the 2- by 2-ft tunnel were completely stripped to accommodate the adaptive-wall test section and its systems. New equipment included the test section, model and angle-of-attack system, laser velocimeter, pressure instrumentation, automated valves for the auxiliary pumps, and computers and electronic instruments required to control this equipment and the existing auxiliary pumps.

Wind Tunnel

The 2- by 2-Foot Transonic Wind Tunnel (fig. 1) is a closed-return tunnel originally designed to operate at Mach numbers up to 1.4 and at total pressures between 0.1 and 3.0 atm. However, because of cracks discovered in the tunnel shell, the adaptive-wall test could only be run at atmospheric pressure. The tunnel is powered by four 1000-hp motors which are mounted inside the pressure vessel and which drive a two-stage, counterrotating compressor.

The adaptive-wall installation is illustrated in figure 2. The test section was mounted between circular upstream and downstream pressure bulkheads and inside a cylindrical shell that sealed the space between the bulkheads. The upstream bulkhead and the pressure shell are omitted in figure 2 so that the test section can be shown more clearly. The pressure shell could be retracted over the downstream bulkhead to allow access to the test section when the tunnel was not operating. A structural box-beam below the test section and a 4-in.-diam pipe above the test section were pressurized by an auxiliary pump; they served as high-pressure-air manifolds. The space inside the pressure shell, which was evacuated by a second auxiliary pump, served as the low-pressure-air reservoir.

A Worthington centrifugal compressor pressurized the high-pressure manifolds to pressures up to 20 lb/in.^{2} higher than the test-section static pressure (p_∞). For the adaptive-wall tests the existing piping was modified to reverse the direction of flow in the pipes leading to the wind tunnel, and a heat

exchanger was added to the discharge leg (fig. 1). With these modifications, air was injected through the slide-valves and withdrawn in the wind-tunnel diffuser. Air discharged from the pump could also return to the pump through a bypass line and valve.

An Allis Chalmers axial-flow compressor maintained the air in the pressure shell at pressures as low as 2 lb/in.^{2} below p_∞. The pump drew air from the pressure shell through a 24-in. line and injected it into the wind-tunnel after-cooler. Most of the air passing through the pump returned directly to the pump inlet through a bypass line and valve.

Test Section

The test section was 2-ft high, 2 ft wide, and approximately 5 ft long. Although the wind tunnel itself had been de-rated from 3 atm operation to 1 atm, the test section was designed for loads at 3 atm. The upper and lower walls were parallel, and there were nine equally spaced longitudinal slots in each. The slots were untapered, open, and extended the full length of the test section. The open area ratio of each wall was 0.13875.

Separate plenums above and below the test section were each divided into 32 compartments by spanwise partitions. The streamwise dimensions of the compartments varied from 1 in. near the model to 4 in. near the ends of the test section (fig. 3). Each compartment contained a loose roll of wire screen to reduce spanwise variations in the flow when high-pressure air was injected.

Pressures in the plenum compartments were controlled by three-way, proportional slide-valves that moved in the spanwise direction along valve seats that formed the backs of the plenums. Two valves are illustrated in figure 4, which is a cross-sectional view of the test section. Each valve was connected to the high-pressure-air reservoir by a flexible hose and to the low-pressure-air reservoir by ports in its upstream and downstream faces. Depending on the position of a valve, ports in its valve seat were either closed to both or open to one of the reservoirs, thus allowing air to be injected into or removed from the test section. Each slide-valve was driven by a stepping motor through a drive-train consisting of speed-increasing chain-and-sprocket,and a ball-screw and nut. In figure 4, the top and bottom valves are in the positions for maximum air injection and removal, respectively.

The sidewalls were formed by 2-in.-thick Schlieren-quality glass windows that were potted into steel frames. The windows were supported at their upstream ends by hinges that allowed them to open outward. Latches in the window frames transferred pressure loads across the windows to angle-irons, which extended between the upstream and downstream bulkheads and defined the outside corners of the test section (fig. 4). A 1.25-in.-diam hole near the center of each window accommodated the model-support shaft.

A single-piece, inflatable rubber seal, glued into a groove in the window frame, was designed to fill the gap between the window frame and the surrounding structure. In operation, however, these seals burst at the window corners, so that for the present tests the junctions between the sidewalls and the upper and lower walls were sealed by small beads of modeling clay pressed into the inside corners of the test section. The upstream and downstream edges of the windows were sealed to the nozzle and diffuser, respectively, by duct tape.

Pressure-relief doors were mounted in the sidewalls immediately downstream of the test section. These doors protected the glass sidewalls from overpressure and under-vacuum in case the auxiliary-pump control system failed. The test section is shown in figure 5 with the pressure shell retracted.

Model and Angle-of-Attack System

The model was a 6-in.-chord NACA 0012 airfoil. It was supported at each end by a 3/4-in.-diam shaft at 30% chord that protruded through the holes in the glass sidewalls. A 0.050-in. gap between each end of the model and the window was filled by a rubber gasket cut to the shape of the airfoil. Lift and drag loads were transferred from the model to the glass through spherical bearings that fit over each end of the shaft and were supported by cups potted into the holes in the windows. Pitching and bending moments were transferred to the window frames by the angle-of-attack mechanism described below.

The model was constructed of stainless steel and had 22 upper-surface and 23 lower-surface pressure orifices along its mid-span. The maximum deviation of the model contour from the theoretical shape at the mid-span was 0.0048 in. Stainless steel pressure leads from the orifices were routed through 1/4-in.-diam holes in the centers of the model support shafts. All tests were conducted without a boundary-layer trip.

The angle of attack was set by two identical mechanisms, one attached to each end of the model shaft (fig. 3). Each mechanism was driven by a stepping motor that was supported in a pivoting bracket; the pivoting bracket was mounted to the window frame and was fitted with a fail-safe brake and a mechanical encoder. Angle of attack was zeroed with a calibrated gunner's quadrant to an accuracy of better than 0.067°. This uncertainty was about twice the resolution of the gunners' quadrant and was due to the uncertainty in establishing the model chord line. Nonzero angles of attack were determined from the geometry of the mechanism.

Laser Velocimeter

The laser velocimeter, illustrated schematically in figure 6, was a two-component, on-axis, forward-scatter system. The light source was a 5-W argon-ion laser. The laser and most of the optics were mounted on a stationary optics table in the control room. The transmitting and collecting lenses were mounted on two-dimensional positioning mechanisms (scanners) that were contained within the pressure vessel. Light from the optics table passed through a 4-in.-diam window in the pressure vessel and was directed to the transmitting lens by a series of turning mirrors on the transmitter scanner.

Optical design– The optical design of the laser velocimeter was unusual because it included a retro-reflector that returned forward-scattered light to the transmitting lens much as if the light had been directly backscattered. This arrangement exploited the much higher signal strength of a forward-scatter system compared with that of a backscatter system, and it was much less sensitive to misalignment between the transmitting and collecting lenses than conventional, off-axis, forward-scatter systems. In addition, the color-separating optics and the photomultiplier tubes could be mounted on the stationary optics table, as in a backscatter system, instead of on the scanning mechanism that carried the collecting lens, where they would have been subjected to high accelerations and vibration.

Because the path length from the laser to the transmitting lens was different at each measurement point, the interference fringes were slightly distorted for all pathlengths but one (where the "waists"—minimum diameters—of the incident beams were at the back focal point of the transmitting lens; cf. ref. 17). The focus of a 1.1 magnification telescope at the laser exit was adjusted so that minimum fringe distortion occurred at a measurement point near the model.

Traversing mechanisms (scanners)– Separate scanners carried the transmitting and collecting lenses. The scanners were supported between the bulkheads on opposite sides of the test section and inside the pressure vessel (fig. 4). Measurements could be made at virtually any point in the plane midway between the sidewalls of the test section. Because alignment had to be maintained over more than 4 ft of travel, the scanners were very stiff. The moving elements were driven along rails by ball screws turned by dc motors. Optical encoders mounted to the motor shafts provided feedback to the scanner control system. Redundant limit switches at the ends of each axis protected the scanners from overtravel.

Alignment system– A unique feature of the laser velocimeter was a computer-controlled alignment system. This was necessary because the optics on the scanners were inaccessible when the pressure shell was closed. Although the alignment system could be operated while the tunnel was running, it was intended for fine-tuning the alignment at the beginning of each shift.

The alignment system performed three functions: (1) it adjusted the angles of the turning mirrors on the transmitter scanner so that the laser beams in transit from the optics table to the transmitting lens were parallel to the mechanical axes of the scanner; (2) it established the position of the laser beams with respect to the test section; and (3) it aligned the collecting lens with respect to the transmitting lens. The angles of the turning mirrors were adjusted remotely by motorized micrometers; beam positions were measured by United Detector Technology position-sensing photodetectors.

A position detector was mounted behind each turning mirror on the transmitting scanner; figure 7 shows a typical installation. The back of each mirror had been polished and a hole cut in its mount so that the transmitted component of one of the four laser beams incident on the mirror could emerge and strike the detector. The face of each detector was a square with 0.39-in. sides. Each detector produced x-y output voltages proportional to the position of the beam on its face. One-inch-diameter polarizing filters were mounted in front of all the detectors, thus allowing the intensities of the beams incident on all the detectors to be adjusted to a common level. A procedure was developed whereby the motorized micrometers were adjusted until the x-y outputs of the detectors remained unchanged (within a small tolerance) over the range of scanner movement.

Detectors, whose positions relative to the test section were accurately known, were mounted to the test-section window frames and used to establish the positions of the laser beams relative to the test section. These are visible in figure 5. A detector was also mounted behind the turning mirror on the receiver scanner and was used to align the collecting lens to the transmitting lens (fig. 6).

Signal processing and data reduction– The amplified output of each photomultiplier tube was presented to a counterstyle signal processor. For each validated signal, the processor output a bin number equal to the number of 1-GHz clock cycles that elapsed in the course of eight cycles of the input signal.

One hundred samples of each channel were acquired at each location. The raw data were then transferred to the "host" computer across a digital input/output (I/O) interface. The host computer reduced the data by first constructing histograms of the bin numbers and then filtering the data by eliminating samples separated from the peak of the histogram by more than one empty bin. The bin numbers of samples that passed this test were then converted to velocities, and the mean and root-mean-squared (rms) values of the resulting velocity distributions were computed.

Calibration– The spacing of the green interference fringes, which measured vertical velocity, was computed from the angle of intersection of the transmitted laser beams (ref. 17). The misalignment between the green fringes and the free-stream direction was estimated by measuring the vertical velocity distribution along the axis of symmetry of the test section, $z/c = 0$, where the vertical velocity was assumed to be zero. These measurements were made with the model installed at zero incidence and with all the slide-valves closed.

The spacing of the blue fringes (used to measure axial velocity) was determined by comparing axial velocity distributions measured by the velocimeter at several Mach numbers with velocities determined from a static pressure pipe that was installed along the centerline of the otherwise empty test section. The fringe spacing determined in this way differed by less than 1% from the theoretical spacing.

Seeding– Tests were run with and without artificial seeding. Without-seeding data rates were typically 50-70/sec immediately after the wind-tunnel main drive was turned on and decreased with time. The naturally occurring seed material was vaporized oil from the main-drive motors. An ultrasonic seeder was installed that injected light mineral oil through a nozzle mounted on the tunnel centerline in the settling chamber upstream of the test section. Although data rates initially increased when the flow was seeded, the gain was eventually offset by a reduction in signal-to-noise ratio as a thin oil film developed on the windows.

Accuracy and repeatability– The measurement volume was about 0.0138 in. in diameter and 0.80 in. long and it could be positioned with an accuracy of about 0.001 in. At Mach 0.80 the counter processors could resolve velocity differences of about 0.004U in both the axial and vertical directions. The rms's of the filtered histograms were typically about 0.010U. Measurements of entire velocity distributions could be repeated with an rms difference of about 0.002U (vertical) and 0.010U (axial).

Pressure Instrumentation

Pressures in all 64 plenum compartments were measured by 16 pneumatic multiplexers, half with ± 1.0-lb/in.^{2} and half with ± 2.5-lb/in.^{2} differential pressure transducers. Flexible plastic tubing connected orifices in the plenum compartments to the multiplexers. Compartments nearest the model were connected to the higher-range transducers. Model and pressure-pipe (used during test-section calibration) pressures were measured by three additional pneumatic multiplexers with ± 15-lb/in.^{2} differential pressure transducers.

Signal conditioning was accomplished using a 32-channel pre-programmable-amplifier-filter unit (PPAFU). The filtered and amplified signals were presented to a Tustin analog-to-digital (A/D) converter, which was interfaced to the host computer. The accuracy of the measurements was better than 1% of the range of the transducers.

Tunnel total temperature and pressure were measured in the settling chamber upstream of the test section. Test-section static pressure was measured at an orifice in the sidewall just upstream of the test section. These pressures and the transducer reference and calibration pressures were measured by Paroscientific absolute pressure transducers. The digital outputs of these instruments were connected to the digital I/O of the host computer.

Computers and Control Systems

The test-section data and control system is illustrated schematically in figure 8. Two computers controlled the test section. The wind-tunnel host computer was a Data General Eclipse S/200 minicomputer. It executed programs that included the logic for measuring and assessing wall interference and for adjusting the plenum pressures. A Hewlett Packard (HP) 9845 desktop computer was interfaced to the test-section hardware; it received its instructions from the host computer.

The Eclipse and HP computers were connected to each other through a 16-bit digital input/output (DIO) interface. The slide-valve, laser velocimeter, and angle-of-attack systems were each connected to the IEEE 488 interface bus of the HP computer through separate, programmable HP 6942A interfaces (multiprogrammers). The pressure instrumentation was connected directly to the DIO and A/D interfaces of the Eclipse computer (fig. 8).

Slide-valves– The slide-valve control system allowed any combination of the 64 valves to be moved simultaneously, with each valve moving a different distance if desired. The system consisted of 64 identical channels, one for each valve, that were connected to a multiprogrammer and its extenders. The only feedback to the control system came from "home" switches near the end of travel of each valve. Valve motion was limited by mechanical stops at both ends; there were no limit switches.

The reference, or home, position of each slide valve was established by driving the valve to where its home switch changed states. The HP 9845 kept track of the number of steps away from this position all subsequent moves should have taken the valve; after each homing operation, it compared this number with the number of steps it actually took to return the valve to home and alerted the user to any discrepancies.

Laser velocimeter– The host computer initiated LV data acquisition by transmitting to the HP computer the coordinates where data were to be acquired, as well as the desired number of samples of each component (up to 1000) at each point. The HP computer then drove the scanners to the first point and began accepting raw data from the signal processors until the last sample of both channels had been acquired. The HP computer transmitted the raw data to the host computer, which immediately reduced the data, and drove the scanners to the next point where the process was repeated.

The scanners were controlled by four closed-loop Electrocraft dc motor control systems, one for each axis of each scanner. The positions of the scanners were established by limit switches near the ends of travel of each axis. Fail-safe brakes were fitted to the vertical axes of the scanners. The control system was connected to the HP multiprogrammer extenders, and all four axes could be moved simultaneously. Whenever the scanner positions were changed, whether by the move or home function, the HP 9845 closed a shutter located near the output end of the laser to block the laser beam during the move.

The alignment of the laser beams to the scanners was accomplished by driving the motorized micrometers that controlled the angles of the turning mirrors and reading the outputs of beam-position detectors behind the turning mirrors. All of the mirror motors were multiplexed to a single controller and only one motor could be driven at a time. There was no direct feedback about the motor positions. The position-sensing photodetectors were multiplexed to one of two United Detector Technology x-y position monitors. Analog x and y signals from the monitors provided indirect feedback of the motorized mirror-micrometer positions.

Angle of attack– The two angle-of-attack mechanisms were controlled by identical channels of electronics. The stepper-motor power supplies, encoders, brakes, and limit switches were all connected to the HP computer through a multiprogrammer. The computer initiated changes in angle of attack by commanding both motors to turn the same number of steps. The computer compared changes in the outputs of the encoders to insure that the commanded angle change had been produced and that the model was not being twisted. The stepper motors did not have sufficient torque to damage the model even when driving the mechanisms in opposite directions.

Auxiliary pumps– The auxiliary pumps were controlled by a General Electric Series Six computer. There were two independent control loops for each pump. One loop controlled the pressure in the associated reservoir by adjusting a control valve in the pipe connecting the reservoir to the pump; the other controlled the operating point of the pump by adjusting a valve in the pump's bypass loop.

The control valves could not be adjusted quickly enough to prevent the pressures in the reservoirs from exceeding their allowable limits when the positions of all the slide-valves were simultaneously changed by more than about 2% of their range. The slide-valves could be adjusted individually and in pairs, however, without restrictions.

PROCEDURE

The procedure for adapting the test section walls involved three steps: (1) measuring flow conditions along a contour surrounding the model, (2) testing the measurements for compatibility with free-air boundary conditions (interference assessment), and (3) adjusting the test section plenum pressures to improve this compatibility (wall control). A fourth step, estimating wall-induced velocities near the model, was not essential but was included as a way to quantify wall interference.

The procedure used in previous adaptive-wall tests at Ames (ref. 18) was based on measurements of a single component of velocity measured along two contours, whereas almost all other adaptive-wall researchers have used a procedure based on measurements of two components along one contour. Since the 2- by 2-ft test section was equipped with a two-component laser velocimeter, either one- or two-component methods could have been applied with equal ease. A comparative study made before the present tests (ref. 19) showed, however, that there are many reasons to prefer two-component methods if the instrumentation is available for making the extra measurements. Specifically, two-component measurements offer the following advantages: (1) they are more sensitive to wall interference; (2) they can be made at fewer locations; (3) they define free-stream conditions (Mach number and flow angle); (4) they yield more interference information (i.e., both components); and (5) they permit computing

solutions on a closed contour to eliminate truncation errors. Therefore, two-component/one-contour methods were applied in the present tests.

Velocity Measurements

Axial and vertical velocities were measured at 16 points along each of two axial lines, 1.5 chord lengths above and below the model. These lines were as close to the upper and lower walls as measurements could be made, and thus were where the effects of plenum pressure changes could be most easily measured. The points were centered with respect to adjacent pairs of plenum compartments (fig. 3). The angle-of-attack mechanism blocked the laser beams at two of the upstream points below the model, so data there were interpolated.

Interference Assessment

Wall interference was assessed by testing the velocity measurements for compatibility with free-air boundary conditions at infinity. For the nonlifting cases, the contour was assumed to extend upstream and downstream to infinity, thus dividing the infinite region outside the contour ("outer flow") into upper and lower half-planes. The flow in each half-plane was computed by applying one of the measured velocity distributions as a boundary condition along the edge of the half-plane and by using free-air boundary conditions at infinity. The resulting outer-flow solution included the distribution of the second component of velocity along the edge of the half-plane. Computed and measured distributions of the second component were compared and differences between them used as the basis for wall adjustments.

If the outer flow can be represented by the linear Prandtl-Glauert equation, then the free-air relationships between axial and vertical velocity distributions at each measurement level can be expressed in closed form (ref. 20):

$$u_m(x,z) = \frac{1}{\beta\pi}\int_{-\infty}^{\infty} \frac{w_m(\xi,z)}{x-\xi}d\xi \tag{1a}$$

$$w_m(x,z) = \frac{-\beta}{\pi}\int_{-\infty}^{\infty} \frac{u_m(\xi,z)}{x-\xi}d\xi \tag{1b}$$

These relationships implicitly satisfy free-air boundary conditions at infinity, and solutions above and below the model are independent of each other. Furthermore, there are no restrictions on the behavior of the flow inside the contour. The relationships were used to approximate the free-air distribution of each component from the measured distribution of the other. The approximations improved as wall interference was reduced.

One difficulty in applying equations (1a) and (1b) is that velocities cannot be measured beyond the ends of the test section. In the nonlifting cases, which were run first, the integrals were truncated at the farthest upstream and downstream measurement points. As will be seen, this introduced significant errors in some outer-flow solutions. Therefore, for the lifting cases, the contour was assumed to be closed near the ends of the test section. Velocities along the upstream and downstream ends of the

contour were interpolated from data at the end-points of the measurement levels. Since in all lifting cases the flow on the model was attached, the wake was thin and its effect was ignored.

For the lifting cases it was also assumed that the flow inside the contour was the linear superposition of model- and wall-induced flows and that the model was small (i.e., that the assumptions of classical, linear wall-interference theory applied). These assumptions, though restrictive, were more appropriate for the lifting than the nonlifting cases, because the latter were run at lower Mach numbers. They allowed the true, free-air velocity distributions to be computed from the measured velocities in a single step (refs. 21 and 22):

$$u_m(x,z) = \frac{u(x,z)}{2} + \frac{1}{2\beta\pi}\int_c \frac{\left[\beta^2(\eta - z)u(\xi,\eta) + (\xi - x)w(\xi,\eta)\right]d\xi - \beta^2\left[(\xi - x)u(\xi,\eta) - (\eta - z)w(\xi,\eta)\right]d\eta}{(\xi - x)^2 + \beta^2(\eta - z)^2} \tag{2a}$$

$$w_m(x,z) = \frac{w(x,z)}{2} - \frac{\beta}{2\pi}\int_c \frac{\left[(\xi - x)u(\xi,\eta) - (\eta - z)w(\xi,\eta)\right]d\xi + \left[\beta^2(\eta - z)u(\xi,\eta) + (x - \xi)w(\xi,\eta)\right]d\eta}{(\xi - x)^2 + \beta^2(\eta - z)^2} \tag{2b}$$

Note that the solutions above and below the model are coupled. Unlike equation (1), all of the velocities on the right-hand side of equation (2) are measured (i.e., the sum of the model- and wall-induced velocities).

Wall Control

The objective of the wall-control phase of the procedure was to adjust the slide-valves in a way that would reduce differences between theoretical and measured velocities at the measurement levels. A linear relationship was assumed between velocity changes at the measurement points and pressure changes in the plenum compartments. The constants of proportionality, or influence coefficients, were measured as part of the calibration of the test section. The resulting influence-matrix and the desired velocity changes were then used to solve (either exactly or approximately) for the necessary plenum pressure changes. The problem was then to adjust the slide-valves to produce these pressure changes.

Adjacent slide-valves were paired, and the valves in each pair were adjusted in unison as if they were a single control. This was done to save time, because, as explained below, the wall controls had to be adjusted one at a time. Although in all cases free-air solutions were computed for both components of velocity, wall-control was always based on differences between measured and theoretical vertical velocity distributions. We chose to control vertical rather than axial velocities because of our experience in running the pilot tests and because of the intuitive relationship between plenum pressure and upwash.

Influence-coefficients– The influence-coefficients were measured by systematically adjusting each slide-valve pair to positions between fully open to the low-pressure reservoir (–100%) to fully open to the high-pressure reservoir (100%) with all other valves closed (0%). At each setting, velocities at the

measurement levels and pressures in the plenum compartments were measured and compared with corresponding measurements made with all valves closed. The change in velocity at each point was plotted versus the change in pressure in the "active" compartments (i.e., the compartments whose valves were adjusted). Since the pressure changes in each pair of active compartments were generally different, the influence-coefficients were defined in terms of pressure changes in the farthest-upstream compartment of each pair. Separate influence-coefficients were determined for air injection and air removal. Each was defined as the slope of the line passing through the origin that best fitted the positive and negative pressure-change data, respectively. Influence-coefficients were measured at Mach 0.75 with the model installed at zero incidence.

It was not possible to isolate the effects of pressure changes in a single plenum compartment, because as each slide valve was adjusted, pressures in many plenum compartments changed. Therefore, the influence-coefficients were defined in terms of "self-induced" pressure changes, that is, the pressure change in each compartment produced by adjusting only its associated slide valve. However, use of this definition required that the wall controls be adjusted one at a time during the wall-control phase of the procedure; otherwise it would have been impossible to distinguish self-induced pressure changes from pressure interactions.

Pressure-change calculation– Based on the results of previous tests (ref. 12), pressure adjustments in the upper plenum were assumed to have little effect on velocities at the measurement level below the model and likewise for the effect of lower-plenum adjustments on velocities at the upper level. This allowed upper and lower plenum pressure changes to be computed independently of each other. Therefore, velocity changes at the 16 points at each measurement level were related to the pressure changes in the 16 pairs of compartments of the corresponding wall by an influence matrix:

$$\begin{pmatrix} \Delta w_1 \\ \vdots \\ \Delta w_{16} \end{pmatrix} = \begin{pmatrix} c_{1,1} & \cdots & c_{1,16} \\ \vdots & \ddots & \vdots \\ c_{16,1} & \cdots & c_{16,16} \end{pmatrix} \begin{pmatrix} \Delta p_1 \\ \vdots \\ \Delta p_{16} \end{pmatrix} \tag{3}$$

This is a square set of equations that could be solved exactly, for example, by Gaussian elimination.

Elements of the exact solution to equation (3) were typically large numbers of alternating sign that were not physically meaningful. Therefore, using the least-squares method of Lawson and Hanson (ref. 23), solutions were computed that only approximately satisfied equation (3), but whose norms were much smaller and whose elements varied more smoothly than those of the exact solution.

Slide-valve adjustments– The slide-valve pairs were adjusted one at a time beginning at the upstream end of the test section and working downstream. Before each pair was adjusted, the pressure in the upstream compartment of that pair was measured, and subsequent pressure changes were computed relative to this pressure. A Newton zero-finding algorithm was then used to adjust the valve pair until the

required pressure change was produced (within an acceptable tolerance) or until 10 valve positions had been tried. The procedure was then repeated for each successive pair of slide valves.

Since the effect of most of the slide-valve adjustments was to relieve tunnel blockage, the free-stream Mach number generally increased as the valves were being adjusted. The desired free-stream Mach number was restored only after the last pair of slide-valves had been adjusted.

WIAC Methods

Wall interference was quantified using a linear wall-interference assessment and correction (WIAC) method to compute wall-induced velocities along the tunnel centerline from each set of velocity measurements. Like the one-step outer-flow solutions discussed above, this method is based on linear wall-interference theory. The wall-induced velocities were computed by using the following expressions, which assume a closed contour (refs. 21 and 22):

$$w_w(x,0) = \frac{\beta}{2\pi}\int_c \frac{[(\xi - x)u(\xi,\eta) - \eta w(\xi,\eta)]d\xi + [\beta^2\eta u(\xi,\eta) + (x - \xi)w(\xi,\eta)]d\eta}{(\xi - x)^2 + \beta^2\eta^2}$$

$$u_w(x,0) = \frac{-1}{2\pi\beta}\int_c \frac{[\beta^2\eta u(\xi,\eta) + (\xi - x)w(\xi,\eta)]d\xi - [\beta^2(\xi - x)u(\xi,\eta) - \beta^2\eta w(\xi,\eta)]d\eta}{(\xi - x)^2 + \beta^2\eta^2}$$

COMPUTER PROGRAMS

Computer programs were written that allowed the user to modify the default flow measurement, interference assessment, and wall-control procedures by selecting from menus of available variations. Once the variations had been selected, the computer automatically executed the procedures without further intervention by the user. It automatically plotted relevant data, such as measured and free-air velocity distributions, slide-valve positions, and model and plenum pressure distributions.

All of the integrals were evaluated numerically assuming linear variation of velocities between adjacent measurement points. Integrals with singularities were evaluated using a limiting procedure described by Everhart (ref. 21). The limits of integration for the infinite-contour integrals (eq. (1)) were the farthest upstream and downstream measurement points.

RESULTS

Test-Section Calibration

Calibration of a conventional test section usually involves measuring variations in Mach number and flow angle along the length of the test section over the range of free-stream conditions for which the test

section was designed. In addition, a method for establishing free-stream conditions must be checked. This kind of calibration is unnecessary in an adaptive-wall test section, because when the wall-adaptation procedure converges to a free-air solution, it automatically eliminates wall-induced flow gradients and unambiguously defines free-stream conditions (ref. 24).

The principal task in the calibration of the present test section was measuring the wall influence-coefficients. Other tasks included measuring the response of the auxiliary-pump control system to slide-valve adjustments, and comparing LV measurements of axial velocity to pressure-pipe data. An important issue that was not investigated was the two-dimensionality of the flow.

Influence-coefficients were measured at Mach 0.75 with the model installed at zero incidence. There was not enough time to measure all the influence-coefficients explicitly. Therefore, the data were generalized by assuming that the influence-coefficients of all compartments of the same size were the same (after accounting for differences between the distances between the compartments and the control points).

Figure 9 illustrates changes in vertical velocity at the measurement level $z/c = 1.5$ for various settings of slide-valves 27 and 28 (operated as a pair with all other valves closed). As expected, suction (negative valve settings) produced an upwash and blowing (positive valve settings) produced a downwash immediately below the active compartments. Furthermore, the magnitudes of the disturbances increased with increased valve openings. This result was typical of all compartment pairs.

In figure 10, the same velocity data are cross-plotted versus pressure changes in compartment 27 (the upstream compartment of the pair). Although the data exhibit considerable scatter, the relationships between pressure and velocity are approximately linear at points where the velocity disturbances were greatest. Each plot includes a straight line passing through the origin that best fits the data in a least-squares sense. The slopes of these lines, defined as the influence-coefficients, are plotted in figure 11 versus axial distance from the control point to the center of the active compartments. Other figures like figure 11 were developed for compartment-pairs of the various sizes and used to generalize the influence-coefficients.

Table 1 presents the influence matrix for the upper wall. Off-diagonal elements within a scatter-band around zero were set to zero. This matrix was used in the adaptive-wall algorithm at all Mach numbers and angles of attack.

Adaptive-Wall Experiments

The adaptive-wall algorithm was applied with the model at angles of attack of 0° and 2° and at free-stream Mach numbers between 0.70 and 0.85. The Reynolds number for all the tests was approximately 2×10^6 (corresponding to atmospheric stagnation conditions). The boundary layer on the model was not tripped and the position of transition to turbulence was unknown. Selected cases are discussed below in the order in which they occurred. The first case (nonlifting) is discussed in considerable detail; data from two subsequent cases are described more briefly. Data from four other cases are not discussed in the text, but are presented without comment in the appendix.

Nonlifting cases– Since both the airfoil (NACA 0012) and walls of the test section were symmetrical, it was assumed for nonlifting cases that the flow field was also symmetrical about the centerline of the test section ($z/c = 0$). Therefore, flow conditions were only measured above the model, and the wall-control algorithm was applied to the upper wall. To maintain flow symmetry, the lower slide-valves were commanded to make the same moves as the corresponding upper valves. Outer-flow solutions were computed from equation (1).

M = 0.80: All of the slide-valves were initially set to –10%, and the low-pressure reservoir setpoint was –1.0 lb/in.^{2} (this was the minimum pressure the Allis Chalmers could produce under these conditions). Slide-valves 1, 13, and 31 were inoperative, so they and the symmetrical lower-wall slide-valves were turned off. Attempts to increase the Mach number to 0.80 with all the valves closed failed because at about $M = 0.77$ the flow in the test section choked.

The initial vertical and axial velocity measurements at $z/c = 1.5$ are compared with their respective outer-flow solutions in figure 12. Each data point includes an error bar that shows the rms of the measurement after filtering. The vertical velocity data indicate that wall adjustments were needed that would increase the upwash upstream of the model and increase the downwash downstream of the model. Intuitively, this would involve increasing suction upstream and decreasing it (or even blowing) downstream. This intuition is consistent with the notion of allowing the streamlines near the wall to pass through it as if the wall were not there.

The axial velocity data (fig. 12(c)) indicated that the peak axial velocities above the model had to be reduced. In the presence of the walls, the model formed a venturi that over-accelerated the flow. The intuitive solution would be to reduce the blockage by increasing wall-suction near the model, thus effectively expanding the channel.

The differences between measured and computed upwashes were multiplied by a "relaxation factor" of less than 1.0 before solving for the plenum pressure changes. For the present case, the relaxation factor was 0.25 for the first two cycles and 0.50 for the final cycle.

Figure 13(a) illustrates the exact solution for self-induced plenum pressure changes computed from the full vertical velocity influence-matrix (table 1) and the desired vertical velocity changes (multiplied by a relaxation factor of 0.25) (fig. 12(a)). Though mathematically exact, the solution clearly violated physical intuition and was the result of the ill-conditioned nature of the problem. Figure 13(b) illustrates an approximate least-squares solution (error norm = 0.002) computed from the same data. This smoother solution, though only approximate, was consistent with physical intuition and was used as the basis for adjusting the slide valves. Note that its norm (0.66) was much smaller than that of the exact solution (3.25). In general, as the approximate solutions became smoother, they also became less accurate.

After the initial wall adjustment, two additional cycles of the adaptive-wall algorithm were executed. The final interference assessment showed that both vertical (fig. 12(b)) and axial (fig. 12(d)) velocity distributions were in much better agreement with their respective outer-flow solutions than they were initially: the rms differences between the measured and computed velocities (rms errors) were approximately half of their initial values. The axial velocity distribution was slightly overcorrected compared with the initial condition, especially near the downstream end of the test section. The failure of the axial velocity measurements to return to zero downstream of the model explains the divergence of the vertical

velocity outer-flow solution at the downstream end of the test section. Figure 14 shows how the rms errors changed with each cycle of wall adjustments.

Figure 15 compares the initial and final slide-valve positions and plenum pressures. Most of the slide-valve adjustments were quite small. Valves upstream of the model were slightly more open to vacuum than they were initially, whereas the vacuum settings of valves downstream of the model had been slightly reduced. Only one valve pair (29-30) had been commanded to move to a pressure setting. Visual inspection of the slide-valves after the test, however, revealed that valve 29 had been malfunctioning and was, in fact, at a very large vacuum setting.

The wall adjustments increased the pressures in most of the plenum compartments, especially those near the model. This is consistent with the reduction in the axial velocities at the measurement level. The pressure data indicate that the initial setting of valve 39 (lower wall) was not at –10% as commanded but at some positive value. The position of valve 40 was also suspect; however, a large reduction in pressure was typical in compartments immediately downstream of a compartment with significant blowing. The final pressure in compartment 29 is consistent with its observed (incorrect) position after the test.

The plenum pressure adjustments moved the shock wave on the model upstream, as if the free-stream Mach number had been reduced (fig. 16). This is consistent with the reduction in peak axial velocities above the model (fig. 12). The WIAC analysis (fig. 17) also showed a reduction in the wall-induced axial velocities with each cycle of wall adjustments. The last cycle produced a substantial overcorrection, but nearly eliminated the streamwise gradient. Since the flow was assumed to be symmetrical, the wall-induced vertical velocity along the tunnel centerline was zero by definition.

In a subsequent nonlifting case, also at Mach 0.80 but starting from slightly different slide-valve settings, the assumption of flow symmetry was checked by measuring velocity distributions below the model, as well as above it. These measurements revealed a flow-angle offset between upper and lower upwash distributions that was initially about 0.5° and that increased to 1.0° after the plenum pressure adjustments. It is likely that there was a similar offset in all the nonlifting cases.

Data for the repeated case at Mach 0.80 and cases at Mach 0.825 and 0.835 are presented in the appendix.

M = 0.85: The initial slide-valve settings for this case were the final settings for the case at M = 0.835 (see fig. 36). As in that case, valves 1, 13, 29, and 31 and the symmetrical lower valves were inoperative. The low-pressure reservoir setpoint was –0.50 lb/in.^{2}. The adaptive-wall algorithm was applied three times using a relaxation factor of 0.25.

Figure 18 shows how the wall adjustments reduced differences between the measured and theoretical velocity distributions at the measurement level. The axial velocity distribution was overcorrected downstream of the model. The figure includes outer-flow solutions computed by solving the transonic small perturbation equation by finite differences (ref. 19). These did not differ significantly from the linear solutions, because the supersonic bubble produced by the model did not extend to the measurement level. As in the case at M = 0.80, the plenum pressure adjustments decreased the rms errors to about half their initial values (fig. 19).

The plenum pressure adjustments progressively reduced the wall-induced axial velocities along the tunnel centerline as illustrated in figure 20. Although the last cycle of wall adjustments overcorrected for wall interference, it yielded a wall-induced distribution that was nearly uniform along the length of the test section. The reduction in effective Mach number moved the shock wave on the model upstream and eliminated flow separation near the trailing edge of the airfoil (fig. 21).

Figure 22 illustrates the initial and final slide-valve positions and plenum pressures. The valves closest to the model were fully open to vacuum after the first cycle of wall adjustments, and subsequent cycles of the algorithm called for further reductions in pressure that could not be produced. Adjustments to valves upstream and downstream of the model were small. No valves were opened to the pressure reservoir. The valve adjustments slightly increased pressures near the model and substantially increased them downstream of the model.

Lifting cases– For the lifting cases the model was set at an angle of attack of 2°, and all the slide-valves were initially closed. Flow measurements were made above and below the model, and outer-flow solutions were computed using the closed-contour, one-step method (eq. (2)). Since the interference of the upper wall was expected to be significantly larger than that of the lower wall, only the top plenum pressures were adjusted; the lower-wall slide-valves remained closed. The relaxation factor for all plenum pressure adjustments was 1.0.

For the $M = 0.70$, $\alpha = 2°$ case and with all valves closed, there were large differences between the measured and theoretical vertical velocities above the model and smaller differences below the model (figs. 23(a) and 23(c)). The measured axial velocities were substantially larger than the outer-flow solutions both above and below the model along the entire length of the test section (fig. 23(e)).

After three cycles of wall adjustments, the measured and theoretical vertical velocity distributions above the model were in substantially better agreement with each other than they were initially (fig. 23(b)). As might be expected, there was no corresponding improvement below the model (fig. 23(d)). The pressure adjustments dramatically improved the agreement between the computed and measured axial velocities both above and below the model (fig. 23(f)). Figure 24 shows the effects of the wall adjustments on the axial and vertical velocity rms errors at the upper measurement level.

Wall-induced axial velocities along the tunnel centerline were all but eliminated by the slide-valve adjustments (fig 25(a)). Moreover, even though the first cycle of adjustments reduced the wall-induced downwashes and their streamwise gradient, the subsequent two cycles had little further beneficial effect and left significant residual interference (fig. 25(b)). The pressure adjustments shifted the shock wave on the model slightly upstream and reduced the suction on the airfoils's lower surface (fig. 26). The normal force coefficient decreased slightly.

Figure 27 illustrates the effect of the slide-valve adjustments on the plenum pressures. A pair of valves immediately upstream of the model, near the position of maximum upwash, was fully open to vacuum. Other valve adjustments were relatively small. Pressures in the upper plenum increased, beginning near the model's leading edge; pressures in the lower plenum also increased and were nearly uniformly equal to the free-stream static pressure.

Even though the one-step interference assessment method was used, three cycles of the adaptive-wall procedure were not sufficient to eliminate interference. This was the same number of iterations that was applied in the nonlifting cases using the iterative interference assessment method. The one-step outer-flow solutions computed before the first plenum pressure adjustments differed little from those computed after the last (fig. 23)—the expected result for a flow that can be represented by the linear one-step theory. This indicates that the rate of convergence to free-air conditions was limited by the accuracy of the wall adjustments rather than by the accuracy of the one-step outer-flow solutions.

DISCUSSION

The data presented above and in the appendix suggest that in all cases the procedure substantially reduced wall interference. In particular, the measured velocity distributions, both axial and vertical, were in much better agreement with the outer-flow solutions after the walls were adjusted than before. In addition, the wall adjustments decreased both the magnitudes and gradients of wall-induced velocities near the model.

The principal effect of the walls was to produce blockage interference, evident as an increase in the local Mach number near the model. This was not surprising since the model was only tested at angles of attack of 0° and 2°. The wall-control procedure relieved this blockage by applying suction in plenum compartments near the model. The pressure adjustments substantially reduced measured axial velocities immediately above and below the model and had relatively little effect on the upwash distributions. In all cases, most of the slide-valves were either closed or partially open to the low-pressure reservoir; very few slide-valves were ever opened to the high-pressure manifold, and those that were were downstream of the model.

Pressure Distribution Comparisons

The plenum pressure adjustments consistently moved the model shock wave upstream of its initial position and eliminated flow separation downstream of the shock wave in those cases in which it occurred. Comparisons of the pressure distributions with numerical data and with data from other wind tunnels show that these changes are consistent with a reduction in wall interference.

The initial and final model pressure distributions for all cases are compared with numerical solutions to the Reynolds-averaged Navier-Stokes equation (ref. 25) in figure 28. The numerical solutions were computed for the model in free air using a Baldwin-Lomax turbulence model and with transition to turbulence fixed at $x/c = 0.05$ on both the upper and lower surfaces. In all cases the experimental data were in much better agreement with the numerical solutions after the walls were adapted than before. In particular, except for the case $M = 0.75$, $\alpha = 2.0$ for which only one cycle of wall adjustments was made (see appendix), the final shock-wave positions were within about 0.05c of the numerical results, and pressure recoveries downstream of the shock waves were in good agreement with the numerical data. In all the nonlifting cases, however, the final experimental pressure coefficients immediately upstream of the shock waves were less negative than in the Navier-Stokes solutions. Exact agreement between the experimental and computational pressure distributions could not be expected, even if the

experimental data were free of wall effects, because the position of transition was fixed in the calculations and unknown in the experiments.

In figure 29 three cases from the present tests are compared with data for the same airfoil acquired in two flexible-wall test sections, the Ames HRC-2 (ref. 26) and the Langley 0.3 Meter (ref. 6). The Langley data were acquired at a slightly higher Reynolds number than were the present data, and the model boundary layer was tripped. The boundary layer on the HRC-2 model was untripped, and free-stream conditions matched those of the present test quite well. (Unlike most adaptive-wall test sections, the wall contours in the HRC-2 were determined from a numerical solution of flow past the airfoil rather than from an outer-flow solution, and the same wall contours were used for a range of test Reynolds numbers. For the data presented in fig. 29, the wall contours were determined for $R = 10\times10^6$, whereas the tests were run at $R = 2\times10^6$.) In both HRC-2 data sets the shock waves were downstream of the positions measured in the 2- by 2-ft wind tunnel; in both Langley data sets the shock waves were farther upstream than in the 2- by 2-ft data.

Reasons for Incomplete Wall Adaptation

The outer-flow solutions, WIAC analyses, and the model pressure distributions all indicate that there was significant residual wall interference after the last cycles of wall adjustments. Among the reasons for the incomplete wall adaptation were the following: (1) the effects of the wall adjustments on the velocities at the measurement points could not be accurately predicted; (2) occasional failure of the slide-valve-setting procedure to produce the required pressure changes in all the plenum compartments; and (3) chronic failure of some of the equipment, particularly the slide-valves.

The influence-coefficients did not accurately represent the relationships between the pressure changes in the plenum compartments and the velocity changes at the measurement level. For example, figure 30 compares vertical velocity changes actually produced by a single cycle of plenum pressure adjustments with those predicted by the influence-coefficients (computed by multiplying the influence matrix by the vector of actual, self-induced plenum pressure changes). At several of the points the velocity actually changed in the direction opposite from what was intended.

A likely reason for the inadequacy of the influence-coefficients was that they were based on over-simplified assumptions that were not explicitly checked. Among these were the assumptions that the effects of pressure changes in all the plenum compartments could be linearly superimposed, that influence-coefficients measured at $M = 0.75$, $\alpha = 0$ could be applied to other test conditions, and that the full matrix could be inferred from measurements of only a few elements. In addition, there was a great deal of scatter in the data from which the influence-coefficients were computed (e.g., figs. 9-11). Thus, even those elements that were measured were not accurately known.

The plenum pressure adjustments were determined in terms of vertical velocity, a quantity that was not particularly sensitive to these adjustments. This also contributed to the difficulty in eliminating wall interference. Differences between the measured and outer-flow vertical velocity distributions diminished mostly because the pressure adjustments moved the outer-flow solutions (which were functions of the measured axial velocity distributions) toward the measured vertical velocities, and not vise versa. A better approach might have been to determine the pressure adjustments directly in terms of axial velocity changes.

Time Required To Adapt The Walls

The minimum time to execute one cycle of the procedure was about 13 min. Most of this time (about 9 min) was spent adjusting the slide-valves. It took about 2.5 min to acquire and reduce the LV data when data rates were at their highest (50-70 samples/sec). The linear interference assessment and plenum pressure change calculations were almost instantaneous, but computer "overhead" items such as storing, retrieving and plotting data consumed almost 2 min.

Wall-adjustment times as short as several seconds could be achieved if (1) a procedure could be developed that allowed all the slide-valves to be adjusted simultaneously and (2) the pump control system could respond quickly enough to prevent pressure transients in the high- and low-pressure reservoirs from exceeding allowable limits. The LV data acquisition times could be reduced to about 60 sec with proper seeding. This is the time it took to scan between the 16 measurement points at each level.

Three-Dimensional Effects

No checks were made of the two-dimensionality of the flow. Before the test section was installed, however, pressure was applied to several of the slide-valves, and the velocity of the air exiting from each of the nine wall slots was measured. Except when the valves were nearly fully open, the velocity distributions were quite uniform (ref. 27). These results are of limited relevance in the present tests, however, because the slide-valves were rarely opened to the pressure manifold.

The thickness of the sidewall boundary layer was not measured so its effect on the flow was unknown.

Improvements Required for Production Testing

The procedure demonstrated in the present tests was clearly unsuitable for production testing. The most serious problems were that it did not completely eliminate wall interference and it took far too long to execute. Less serious were the chronic failures of many of the systems. In particular, the following improvements are needed.

1. A more accurate method must be developed to determine the proper wall adjustments from the velocity data. The method must allow all the slide-valves to be adjusted simultaneously.

2. A method must be developed for seeding the test section without getting the sidewall windows dirty. Ideally the seed would be concentrated in the midplane of the test section at the measurement levels.

3. The reliability of the slide-valve control system must be improved. The stepping motors should be fitted with encoders to provide feedback to the control system.

4. The sidewall window seals must be redesigned.

5. The performance of the auxiliary-pump control system should be improved so that control parameters stay within safe limits during arbitrary slide-valve adjustments. The response time of the

control system could be decreased by using higher-pressure air to drive the pneumatically actuated control valves. The bypass circuit and the control system of the Allis Chalmers pump should be modified to allow the pump to produce lower pressures in the low-pressure reservoir. Lower pressures will be needed for tests at Mach numbers higher than 0.85.

6. The reliability of the Worthington pump must be improved.

CONCLUSIONS

First tests were conducted in a new adaptive-wall test section installed in the Ames 2- by 2-Foot Transonic Wind Tunnel. These tests demonstrated the integrated operation of the test-section systems, including the following: slide-valves for controlling plenum pressures; a fast-scan, two-component laser velocimeter; an auxiliary pump control system; and on-line interference assessment. An automatic procedure for adjusting plenum pressures was demonstrated that consistently reduced wall interference. This conclusion is based on (1) comparisons of measured axial and vertical velocity distributions with the outer-flow solutions, (2) calculations of wall-induced velocities near the model, and (3) comparisons of the model pressure distribution with CFD solutions for the model in free air and with data from other wind tunnels.

The plenum pressure adjustments produced large changes in axial velocities and much smaller changes in vertical velocities near the walls of the test section. This occurred because at the low angles of attack at which the model was tested, blockage interference was much larger than lift interference.

In all cases, significant and measurable interference remained after the adaptive-wall procedures were applied. The foremost reason for this was that the necessary velocity changes at the measurement levels could not be accurately produced. In particular, the influence matrix did not accurately represent the relationships between pressure changes in the plenum compartments and velocity changes at the measurement levels. In addition, pressure adjustments were computed in terms of vertical velocity, which was not sensitive to the adjustments.

Although the plenum pressure adjustments did not eliminate interference, they did substantially reduce the streamwise gradient of the wall-induced flow field, thus making the flows far more "correctable" for wall effects.

Further development of the adaptive-wall test section is required before it will be suitable for production testing. Specifically, the method for determining the proper wall adjustments must be improved, and the time required to execute the procedure must be drastically reduced. Shorter execution times could be achieved by improving the seeding of the laser velocimeter and by developing a wall-control method that allows all the slide-valves to be adjusted simultaneously.

APPENDIX

DATA FOR ADDITIONAL EXPERIMENTAL CASES

The data for four cases—three nonlifting and one lifting—are presented without comment in figures 31 through 38. The cases covered are the following:

1. $M = 0.80$, $\alpha = 0°$ (figs. 31 and 32)

2. $M = 0.825$, $\alpha = 0°$ (figs. 33 and 34)

3. $M = 0.835$, $\alpha = 0°$ (figs. 35 and 36)

4. $M = 0.75$, $\alpha = 0°$ (figs. 37 and 38)

REFERENCES

1. Preston, J. H.; and Sweeting, N. E.: The Experimental Determination of the Interference on a Large Chord Symmetrical Joukowski Aerofoil Spanning a Closed Tunnel. British Aeronautical Research Committee, R&M No. 1997, Dec. 1942.

2. Preston, J. H.; Sweeting, N. E.; and Cox, D. K.: The Experimental Determination of the Two-Dimensional Interference on a Large Chord Piercy 12/40 Aerofoil in a Closed Tunnel Fitted with a Flexible Roof and Floor. British Aeronautical Research Committee, R&M No. 2007, Sept. 1944.

3. Lock, C. N. H.; and Beavan, J. A.: Tunnel Interference at Compressible Speeds Using the Flexible Walls of the Rectangular High-Speed Tunnel. British Aeronautical Research Committee, R&M No. 2005, Sept. 1944.

4. Lewis, M. C.: Aerofoil Testing in a Self-Streamlining Flexible Walled Wind Tunnel. NASA CR-4128, 1988.

5. Chevallier, J. P.; Mignosi, A.; Archambaud, J. P.; and Seraudie, A: T2 Wind Tunnel Adaptive-Walls: Design, Construction and Some Typical Results. La Recherche Aérospatiale (English Edition)(ISSN 0379-380X), no. 4, 1983, pp. 1-19.

6. Wolf, S. W. D.: Evaluation of a Flexible Wall Testing Technique to Minimize Wall Interferences in the NASA Langley 0.3-m Transonic Cryogenic Tunnel. AIAA Paper 88-0140, Reno Nev., 1988.

7. Jiaju, H.; Peichu, Z.; and Huaxing, L.: Experimental Research from Low Speed Two Dimensional Flexible Wall Self Streamlining Wind Tunnels. Hangkong Xuebao, vol. 7, no. 3, 1986, pp. 217-224. (AD-A180 993, trans by F33657-84-D-0165.)

8. Ganzer, U; Igeta, Y.; and Ziemann, J.: Design and Operation of the TU-Berlin Wind Tunnel with Adaptive Walls. Paper 84-2.1.1, 14th Congress of the International Council of the Aeronautical Sciences, Toulouse, France, Sept. 1984.

9. Heddergott, A.; and Wedemeyer, E.: Deformable Adaptive Wall Test Section for Three-Dimensional Wind Tunnel Testing. vol. 1. Paper 84-2.1.2, 14th Congress of the International Council of the Aeronautical Sciences, Toulouse, France, Sept. 1984, pp. 66-75.

10. Erickson, J. C.; Wittliff, C. E.; Padova, C.; and Homicz, G. F.: Adaptive-Wall Wind-Tunnel Investigations. Calspan Report No. 6040-A-2, Buffalo, New York, Feb. 1981.

11. Parker, R. L.; and Sickles, W. L.: Two-Dimensional Adaptive-Wall Experiments. Arnold Engineering Development Center, Arnold Air Force Station, Tennessee, AEDC-TR-80-63, Feb. 1981.

12. Satyanarayana, Bodapati; Schairer, E. T.; and Davis, S. S.: Adaptive-Wall Wind Tunnel Development for Transonic Testing. J. Aircraft, vol. 18, no. 4, Apr. 1981, pp. 273-279.

13. Schairer, E. T.: Experiments in a Three-Dimensional Adaptive-Wall Wind Tunnel. NASA TP-2210, 1983.

14. Parker, R. L.; and Erickson, J. C., Jr.: Status of Three-Dimensional Adaptive-Wall Test Section Development at AEDC. AIAA Paper 84-0624, San Diego, Calif., 1984.

15. Sears, W. R.; and Lee, D. C. L.: Experiments in an Adaptable-Wall Wind Tunnel for V/STOL Testing. University of Arizona, Tucson, Ariz., Grant AF-AFOSR-82-0185, Final Report, Sept. 1986.

16. Celik, Z.; and Roberts, L.: An Experimental Study of an Adaptive-Wall Wind Tunnel. Ames Research Center and Stanford University Joint Institute for Aeronautics and Acoustics TR-87, Aug. 1988.

17. Durst, F.; Melling, A.; and Whitelaw, J. H.: Principles and Practice of Laser Doppler Anemometry. Academic Press, 1981, p. 125.

18. Davis, S. S.: A Compatibility Assessment Method for Adaptive-Wall Wind Tunnels. AIAA J., vol. 19, no. 9, Sept. 1981, pp. 1169-1173.

19. Schairer, E. T.: Methods for Assessing Wall Inteference in the Two- by Two-Foot Adaptive-Wall Wind Tunnel. NASA TM 88252, June 1986.

20. Sears, W. R.: Self-Correcting Wind Tunnels. In: Aeronautical Journal, vol. 78, Feb.-Mar. 1974, pp. 80-89.

21. Everhart, J. L.: A Method for Modifying Two-Dimensional Adaptive Wind-Tunnel Walls Including Analytical and Experimental Verification. NASA TP-2081, 1983.

22. Mokry, M.; Chan, Y. T.; and Jones, D. J.: Two-Dimensional Wind Tunnel Wall Interference. AGARDograph No. 281, Nov. 1983.

23. Lawson, C. L.; and Hanson, R. J .: Solving Least Squares Problems. Prentice Hall, 1974.

24. Sears, W. R.: Adaptable Wind Tunnel for Testing V/STOL Configurations at High Lift. J. Aircraft, vol. 20, no. 11, Nov. 1983, pp. 968-974.

25. King, L. S.: A Comparison of Turbulence Closure Models for Transonic Flows about Airfoils. AIAA Paper 87-0418, 1987.

26. McDevitt, J. B.; and Okuno, A. F.: Static and Dynamic Pressure Measurements on a NACA 0012 Airfoil in the Ames High Reynolds Number Facility. NASA TP-2485, 1985.

27. Morgan, D. G.; and Lee, G.: Construction of a Two- by Two-Foot Transonic Adaptive-Wall Test Section at the NASA Ames Research Center. AIAA Paper 86-1089, 1986.

TABLE 1.– INFLUENCE COEFFICIENTS

LV point	Plenum compartment pair[a]															
	1	2	3	4	5	6	7	8	9	10	11	12	13	14	15	16
1	0.40 (0.45)	0.06 (0.05)														
2	0.20 (0.20)	0.35 (0.39)	0.06 (0.04)													
3		0.18 (0.10)	0.35 (0.39)	0.10 (0.05)												
4			0.21 (0.12)	0.20 (0.30)	0.05 (0.05)											
5				0.05 (0.10)	0.15 (0.31)	0.10 (0.14)										
6					0.15 (0.28)	0.15 (0.31)	0.10 (0.14)									
7					0.07 (0.07)	0.15 (0.28)	0.15 (0.31)	0.10 (0.14)								
8						0.07 (0.07)	0.15 (0.28)	0.15 (0.31)	0.10 (0.14)							
9							0.07 (0.07)	0.15 (0.28)	0.15 (0.31)	0.10 (0.14)						
10								0.07 (0.07)	0.15 (0.28)	0.15 (0.31)	0.10 (0.14)					
11									0.07 (0.07)	0.15 (0.28)	0.15 (0.31)	0.10 (0.14)				
12										0.07 (0.07)	0.15 (0.28)	0.15 (0.31)	0.10 (0.14)			
13											0.07 (0.07)	0.15 (0.28)	0.15 (0.31)	0.05 (0.13)		
14												0.06 (0.07)	0.13 (0.23)	0.15 (0.28)	0.10 (0.15)	0.05
15														0.10 (0.06)	0.25 (0.39)	0.10 (0.10)
16															0.17 (0.15)	0.25 (0.45)

[a]All table values are negative. Vacuum influence-coefficients, (Δw/U)/(Δp/pt), shown open throughout table; pressure influence-coefficients shown in parentheses throughout table.

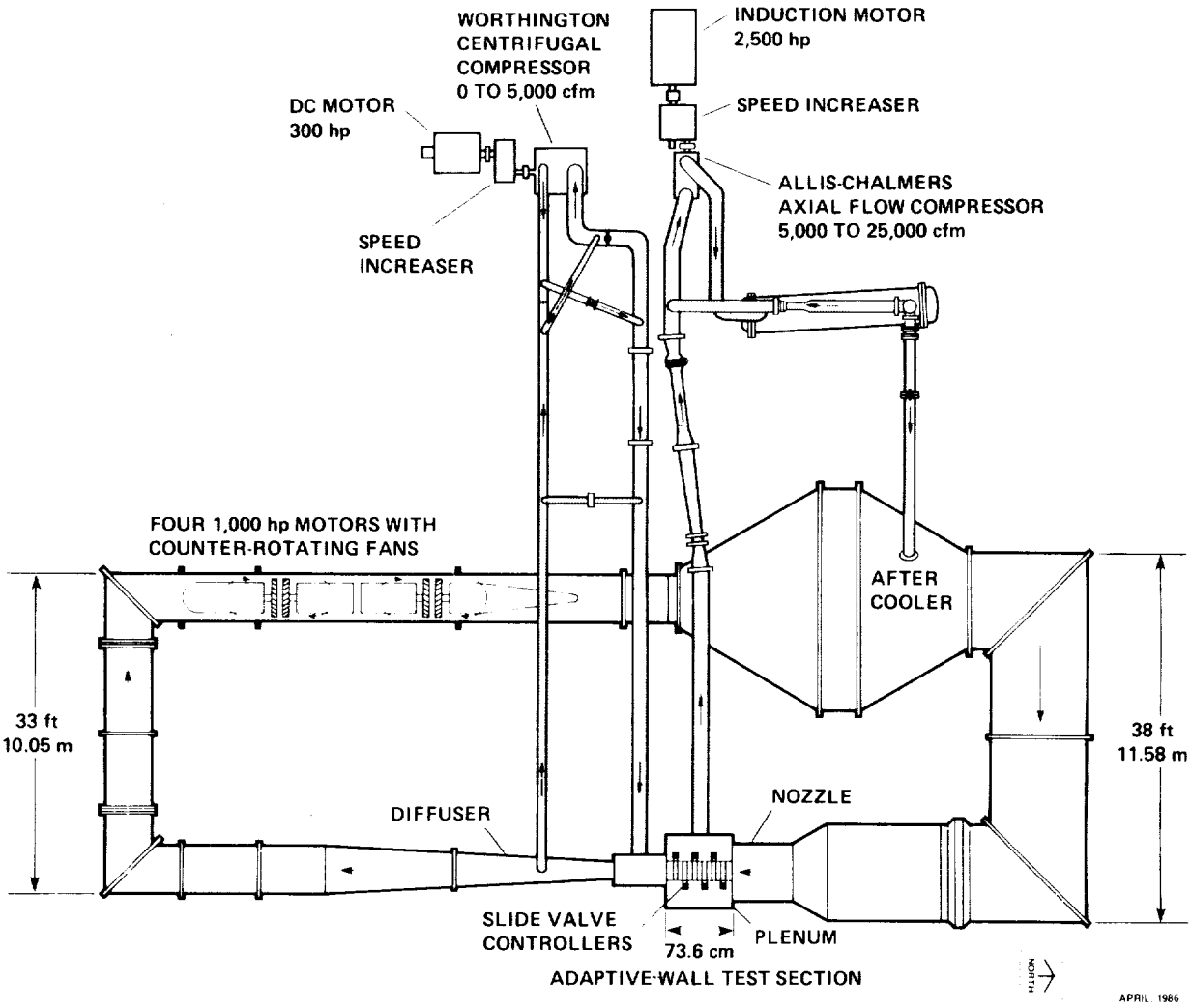

Figure 1.– The Ames 2- by 2-Foot Transonic Wind Tunnel.

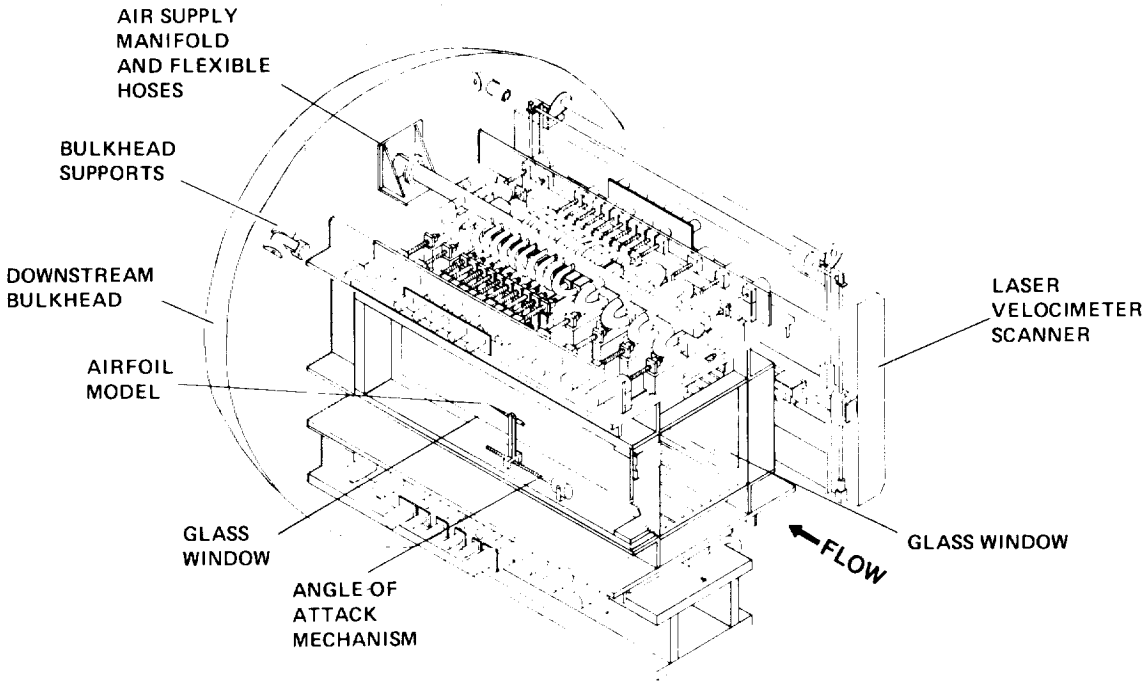

Figure 2.– The 2- by 2-ft adaptive-wall test section.

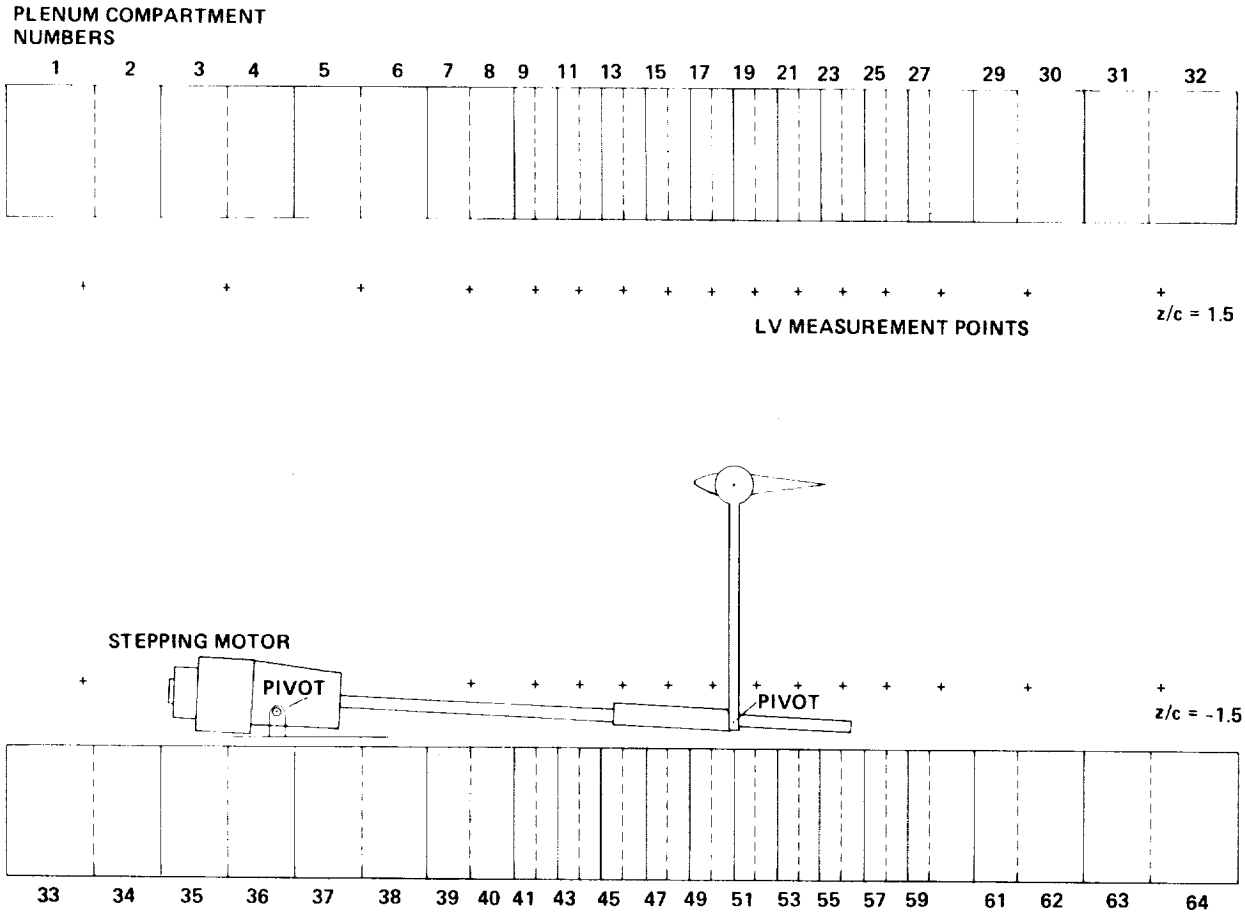

Figure 3.– View of test section showing plenum compartments, LV measurement points, and angle-of-attack mechanism.

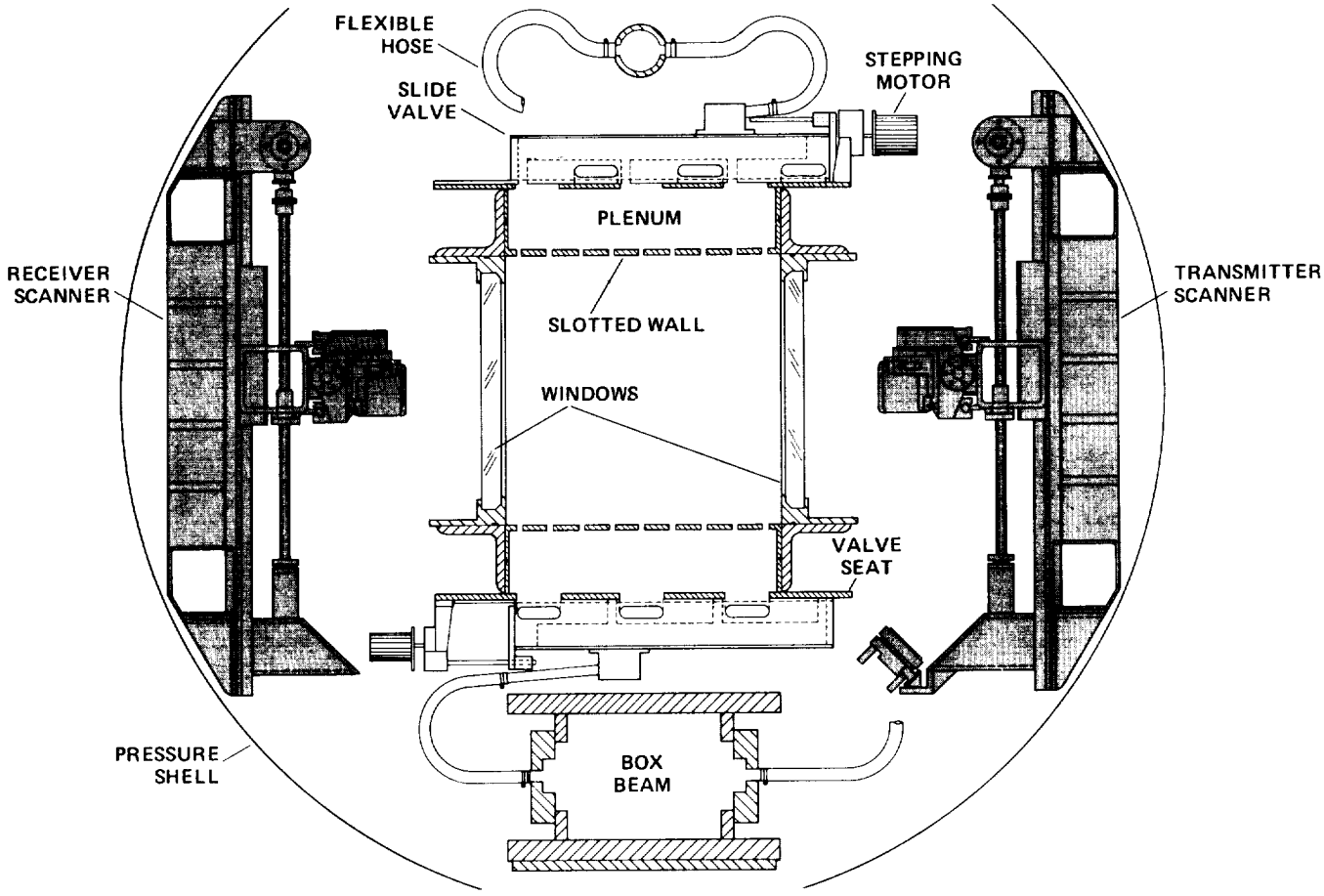

Figure 4.– Lateral cross section of test section.

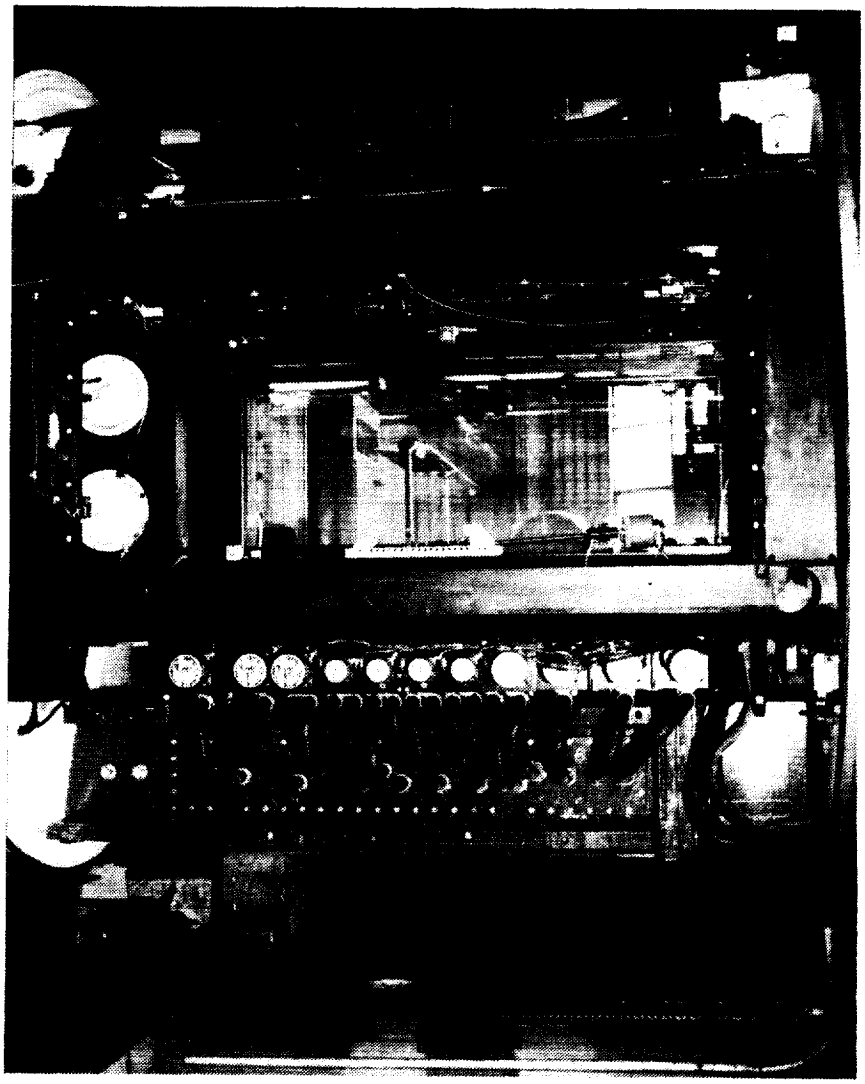

Figure 5.– Test section with model and LV scanners installed.

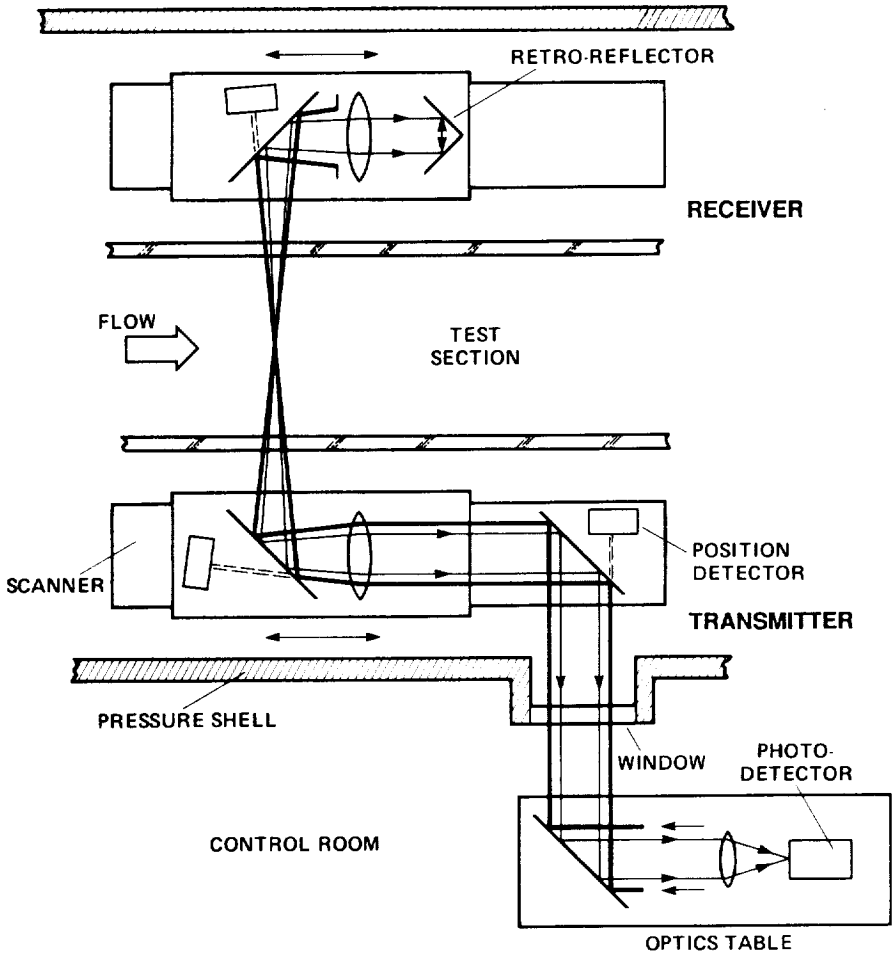

Figure 6.– Schematic of laser velocimeter.

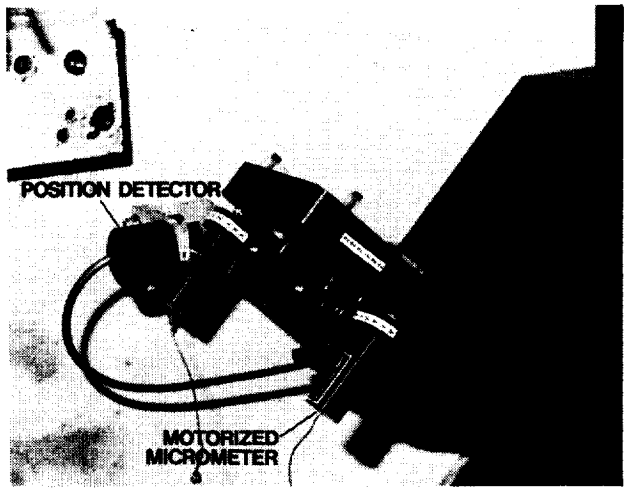

Figure 7.– Turning mirror on the transmitter scanner showing position detector and motorized micrometers.

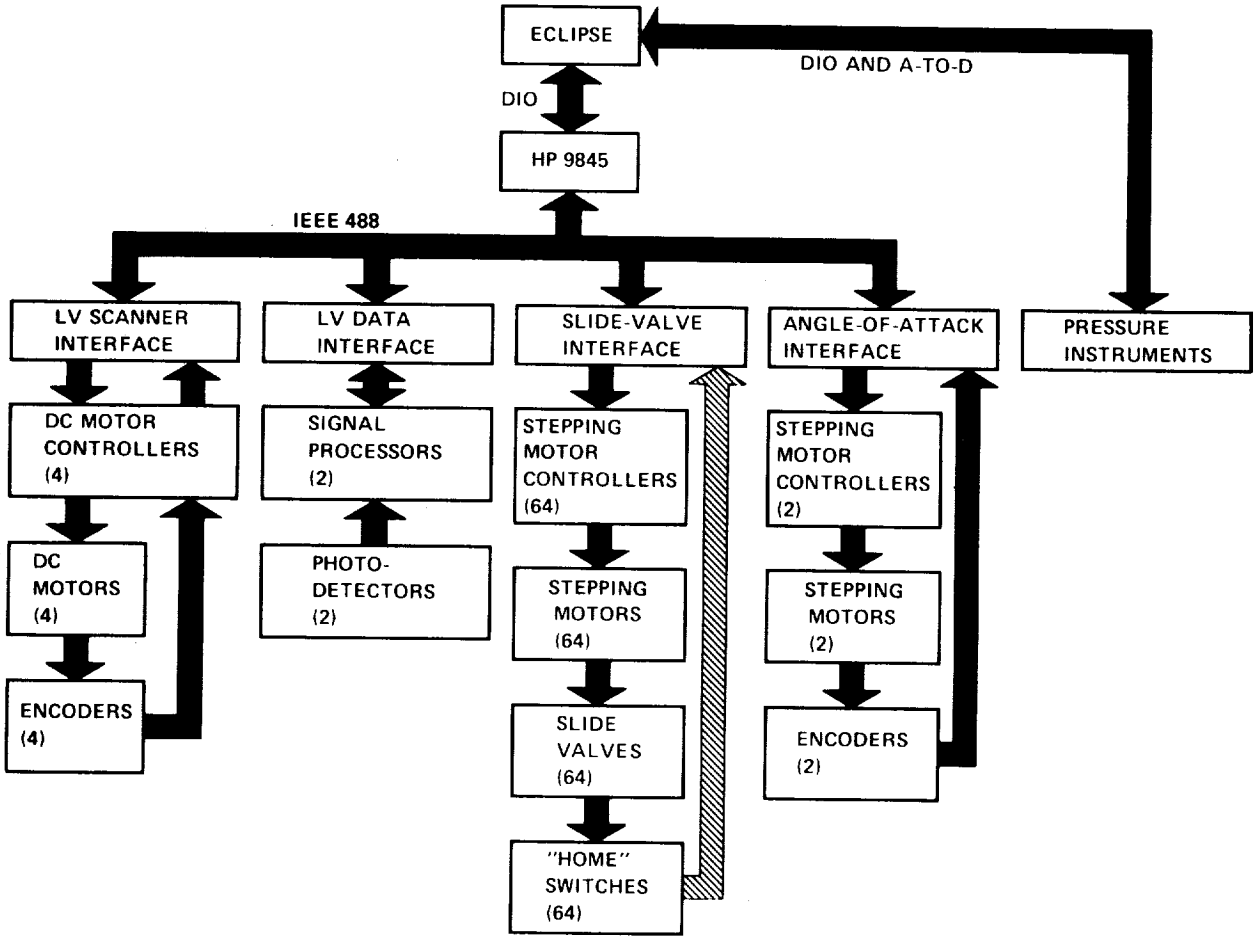

Figure 8.– Schematic of test-section data and control system.

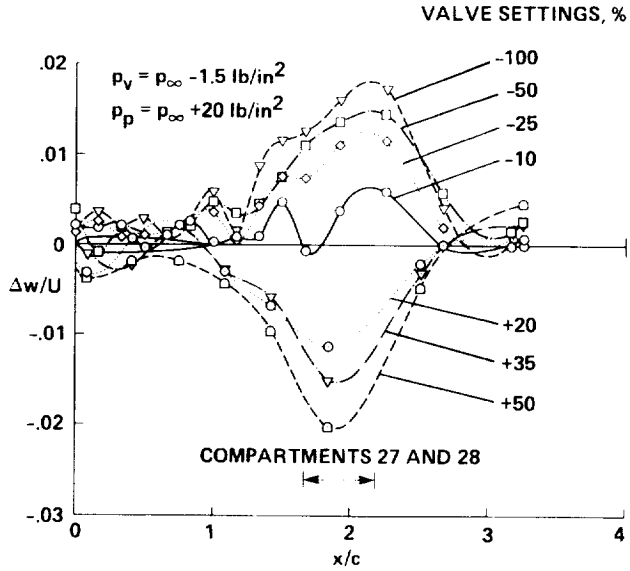

Figure 9.– Changes in vertical velocity at level z/c = 1.5 for various settings of valve pair 27-28.

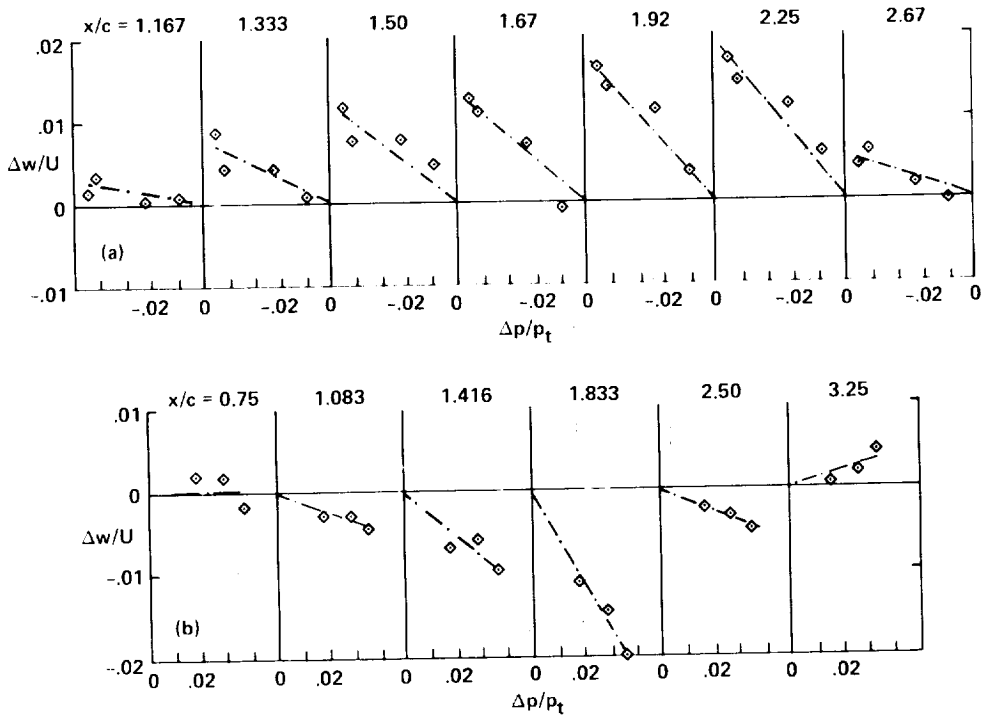

Figure 10.– Velocity changes at level z/c = 1.5 versus pressure changes in plenum compartment 27.

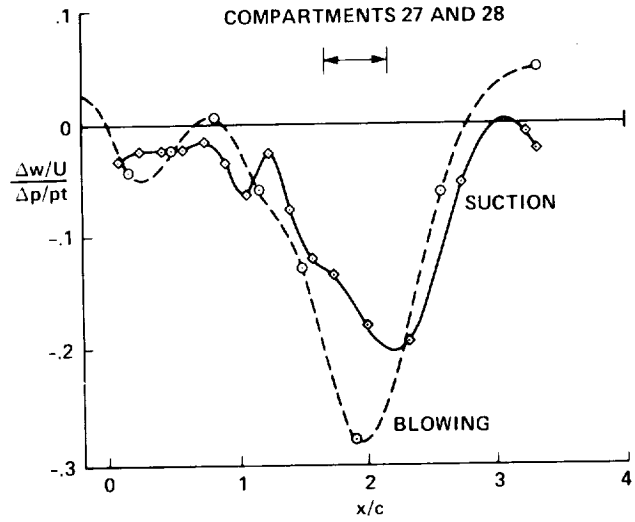

Figure 11.– Influence-coefficients versus axial distance.

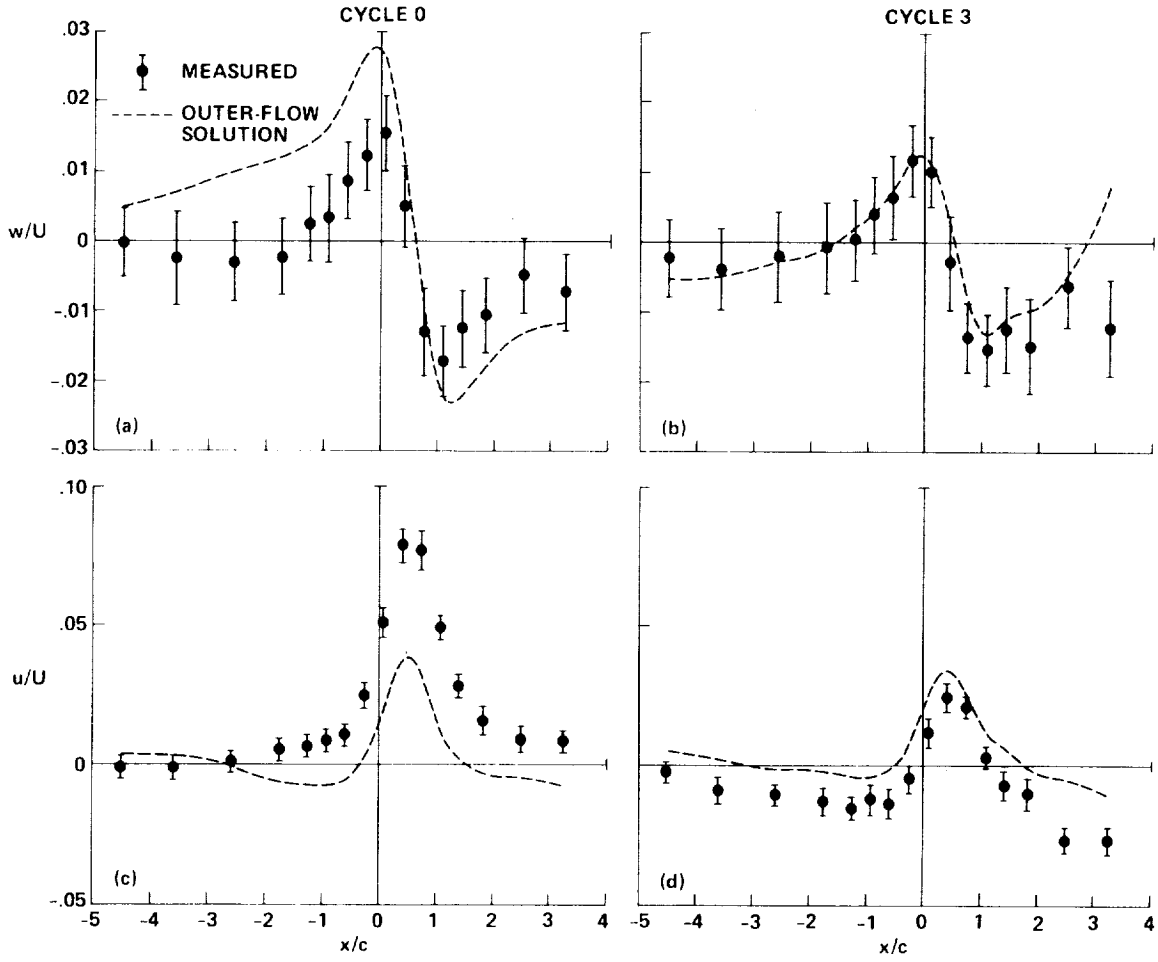

Figure 12.– Comparison of measured velocities with outer-flow solutions before and after wall adjustments: z/c = 1.5, M = 0.80, $\alpha = 0$. (a) Vertical velocity, cycle 0; (b) vertical velocity, cycle 3; (c) axial velocity, cycle 0; (d) axial velocity, cycle 3.

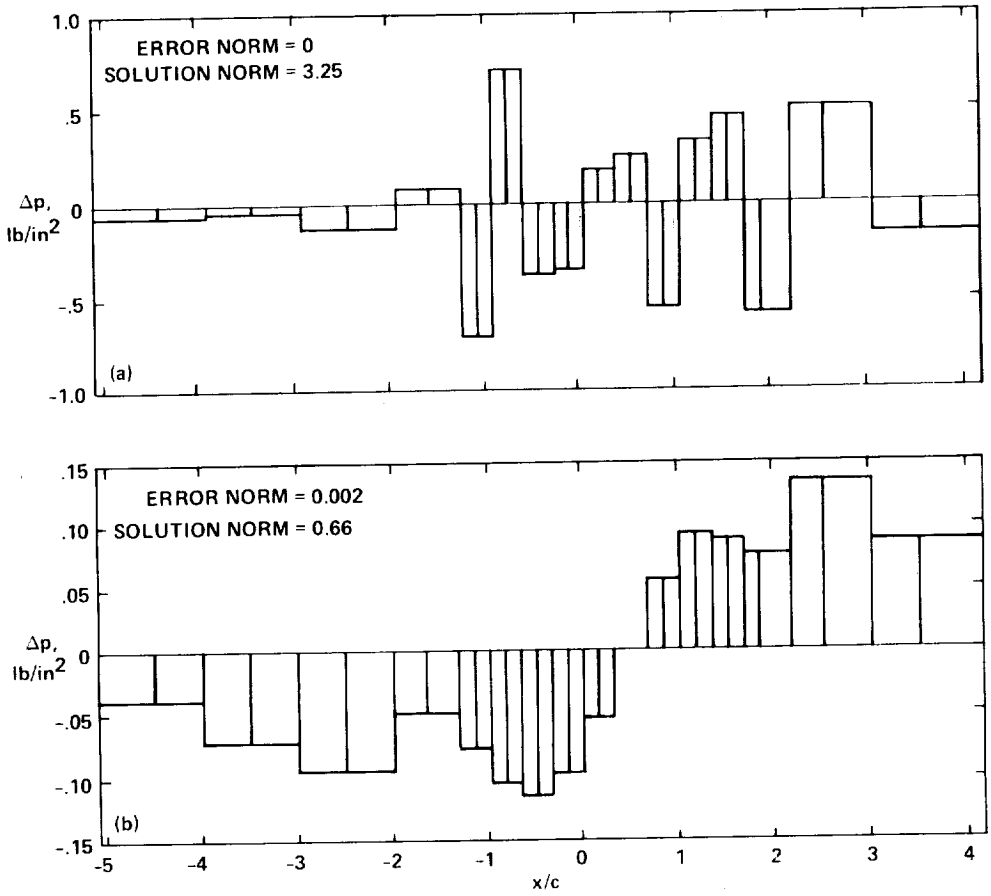

Figure 13.– Exact and approximate solutions for self-induced plenum compartment pressure changes: M = 0.80, $\alpha = 0$. (a) Exact solution (Gaussian elimination); (b) approximate solution (least-squares, ref. 23).

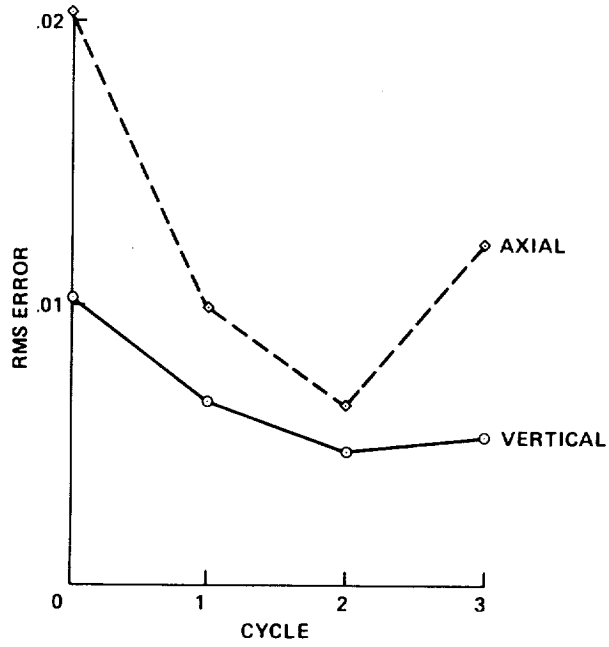

Figure 14.– RMS differences between measured velocities and outer-flow solutions versus iteration number: M = 0.80, $\alpha = 0°$.

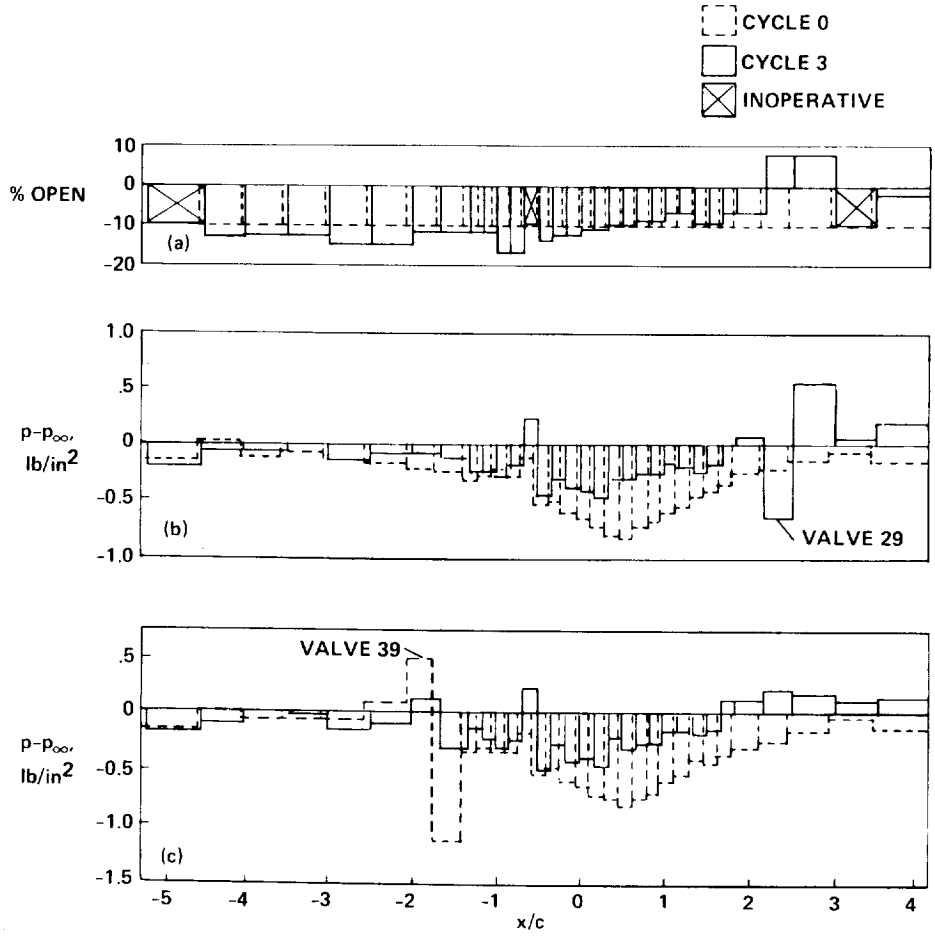

Figure 15.– Comparisons of initial and final slide-valve positions and plenum compartment pressures: $M = 0.80$, $\alpha = 0°$. (a) Slide-valve positions, top and bottom; (b) plenum pressures, top; (c) plenum pressures, bottom.

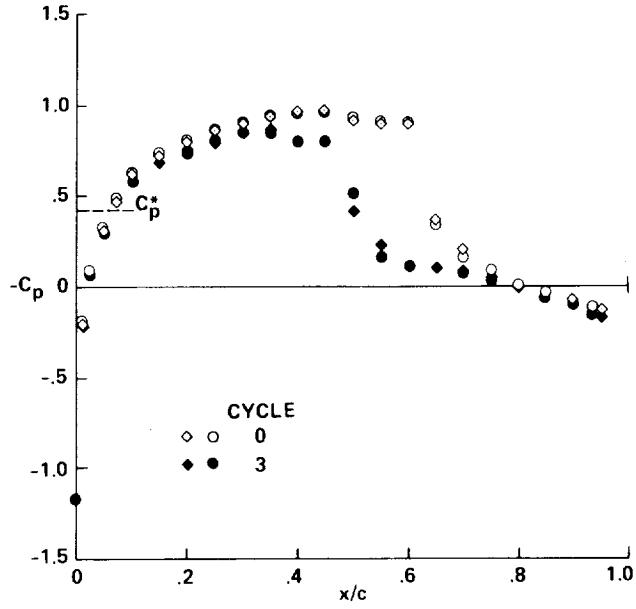

Figure 16.– Effect of wall adjustments on model pressure distribution: M = 0.80, $\alpha = 0°$.

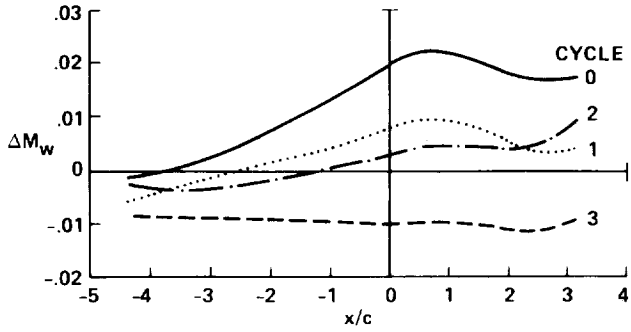

Figure 17.– Effect of wall adjustments on wall-induced Mach number along test section centerline: z/c = 0, M = 0.80, $\alpha = 0°$.

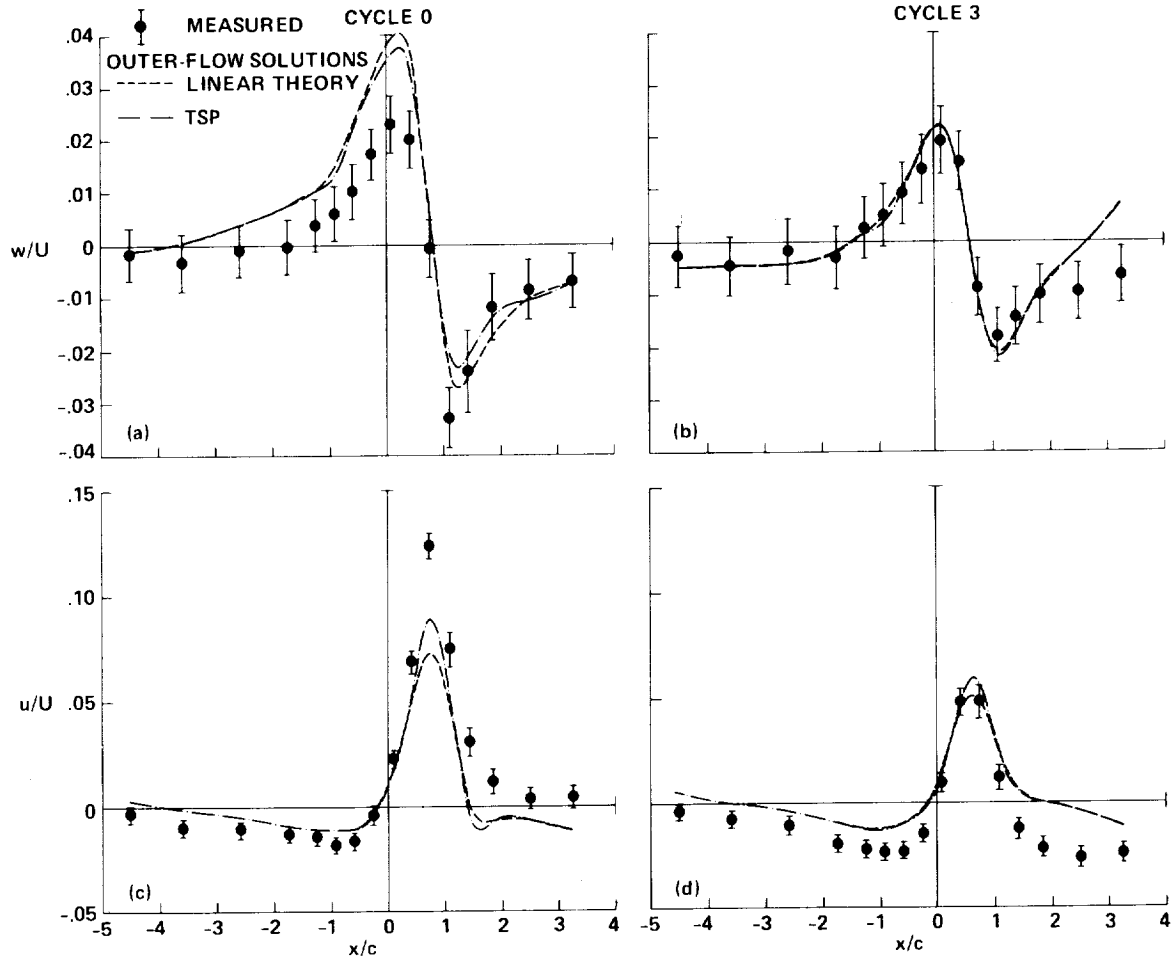

Figure 18.– Comparison of measured velocities with outer-flow solutions before and after wall adjustments: z/c = 1.5, M = 0.85, $\alpha = 0°$. (a) Vertical velocity, cycle 0; (b) vertical velocity, cycle 3; (c) axial velocity, cycle 0; (d) axial velocity, cycle 3.

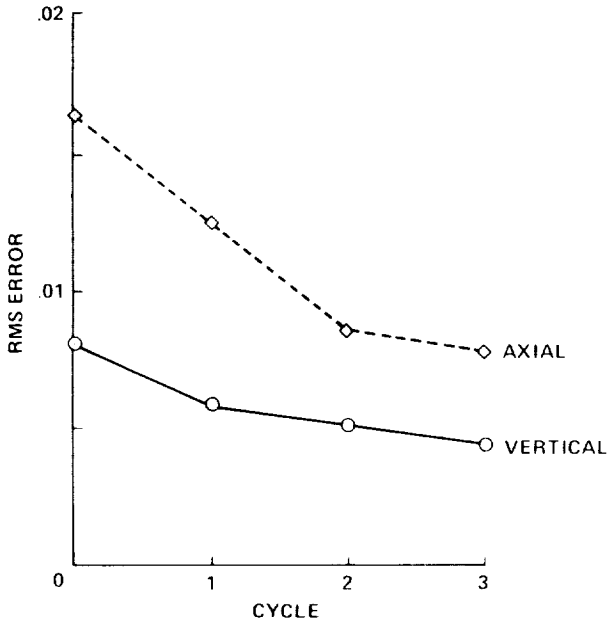

Figure 19.– Effect of wall adjustments on rms differences between measured velocities and outer-flow solutions: M = 0.85, $\alpha = 0°$.

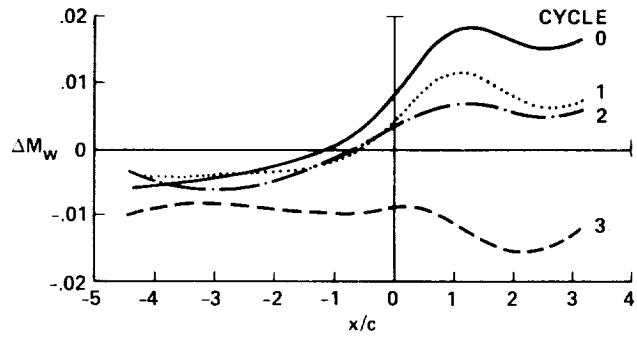

Figure 20.– Effect of wall adjustments on wall-induced Mach number along test-section centerline: z/c = 0, M = 0.85, $\alpha = 0°$.

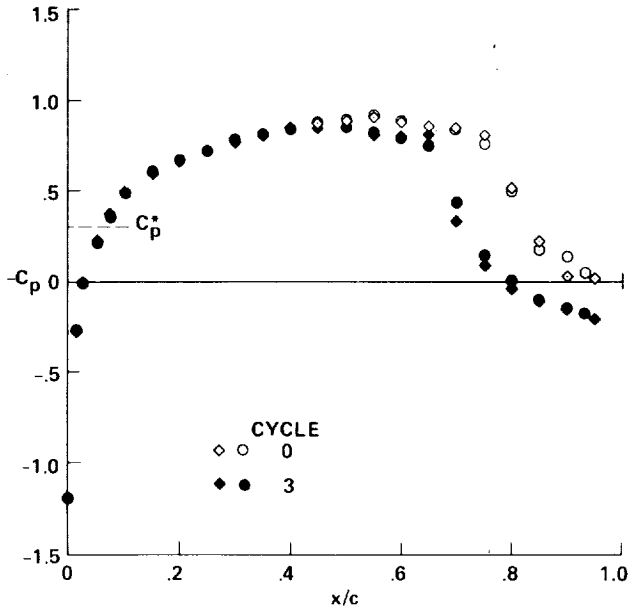

Figure 21.– Effect of wall adjustments on model pressure distribution: M = 0.85, $\alpha = 0°$.

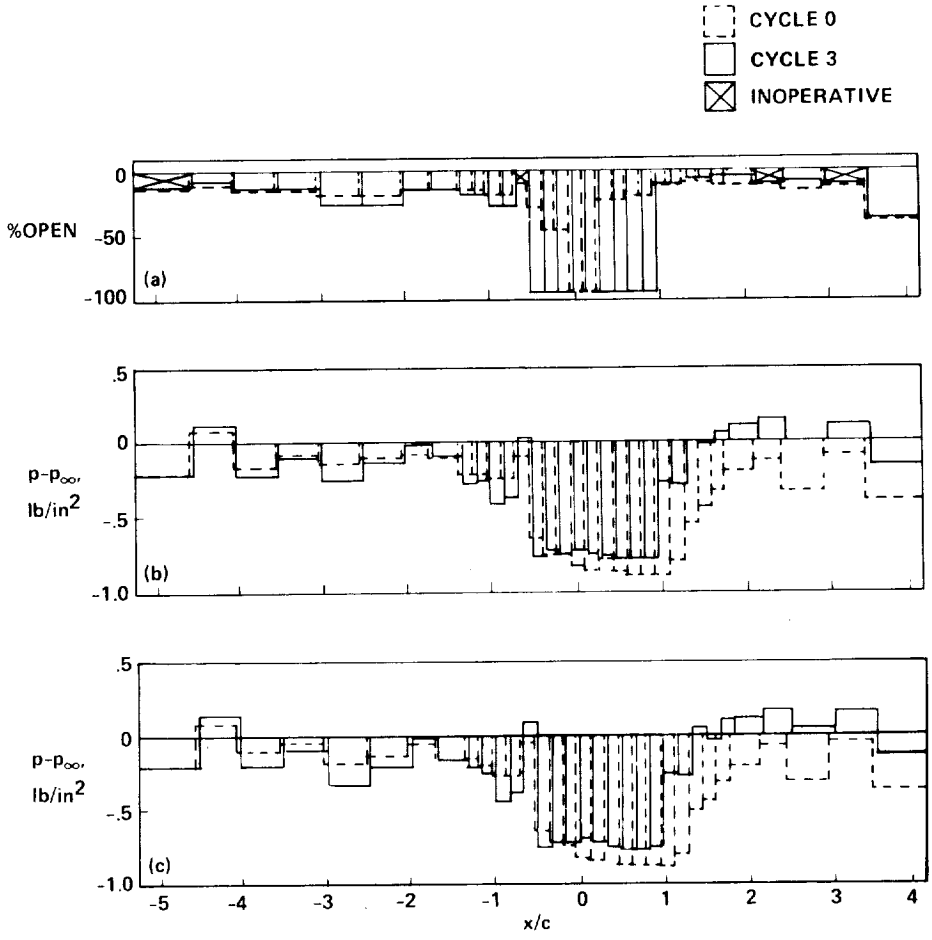

Figure 22.– Comparison of initial and final slide-valve positions and plenum compartment pressures: $M = 0.85$, $\alpha = 0°$. (a) Slide-valve positions, top and bottom; (b) plenum pressures, top; (c) plenum pressures, bottom.

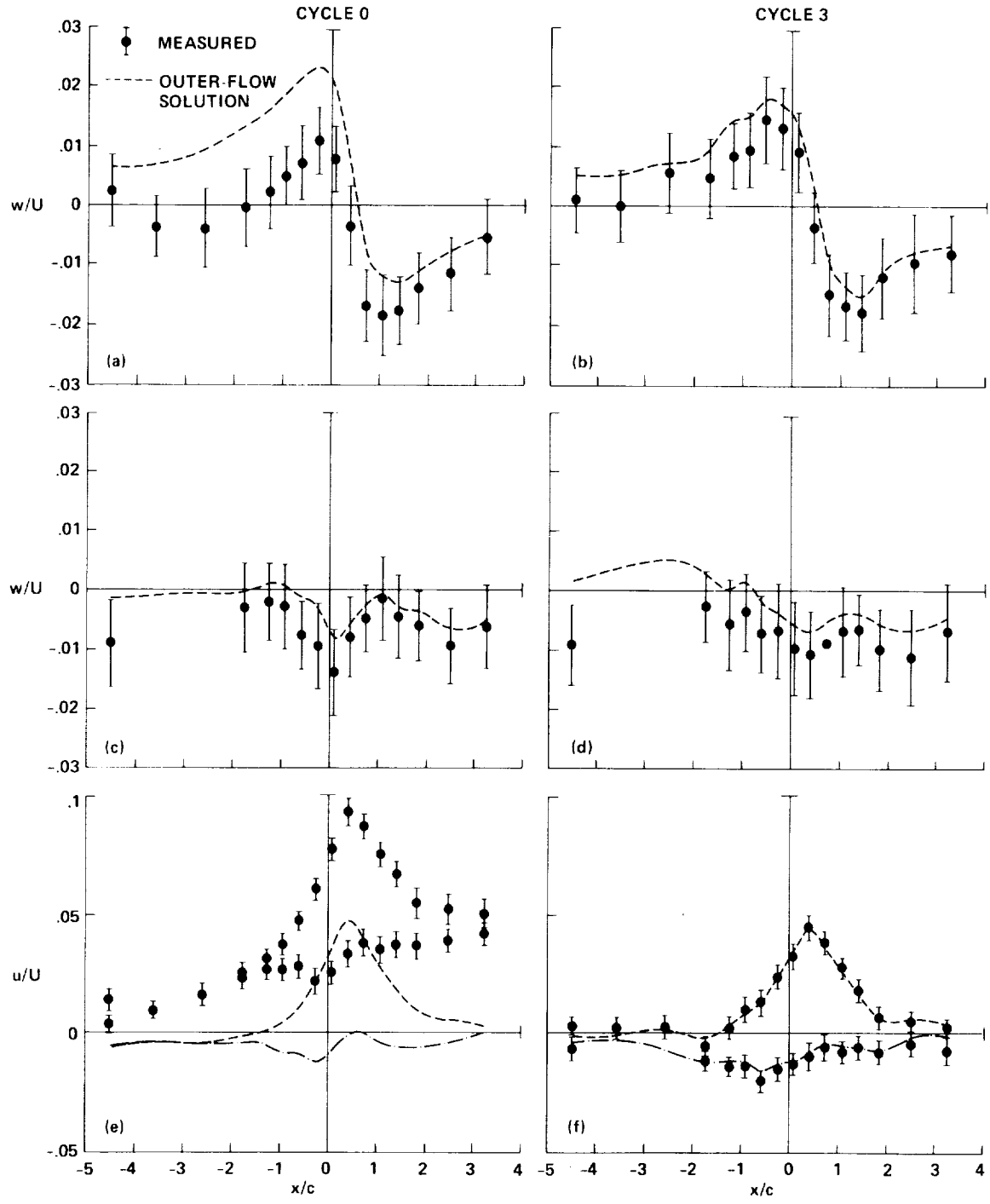

Figure 23.– Comparison of measured velocities with outer-flow solutions before and after wall adjustments: M = 0.70, $\alpha = 2°$. (a) Vertical velocity, z/c = 1.5, cycle 0; (b) vertical velocity, z/c = 1.5, cycle 3; (c) vertical velocity, z/c = –1.5, cycle 0; (d) vertical velocity, z/c = –1.5, cycle 3; (e) axial velocity, z/c = ±1.5, cycle 0; (f) axial velocity, z/c = ±1.5, cycle 3.

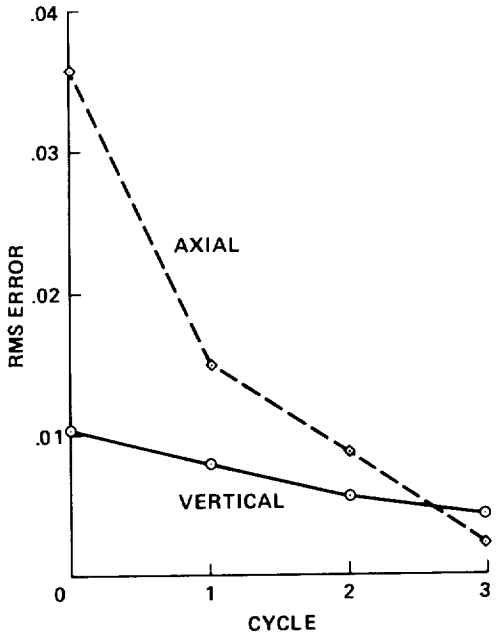

Figure 24.– Effect of wall adjustments on rms errors: M = 0.70, $\alpha = 2°$.

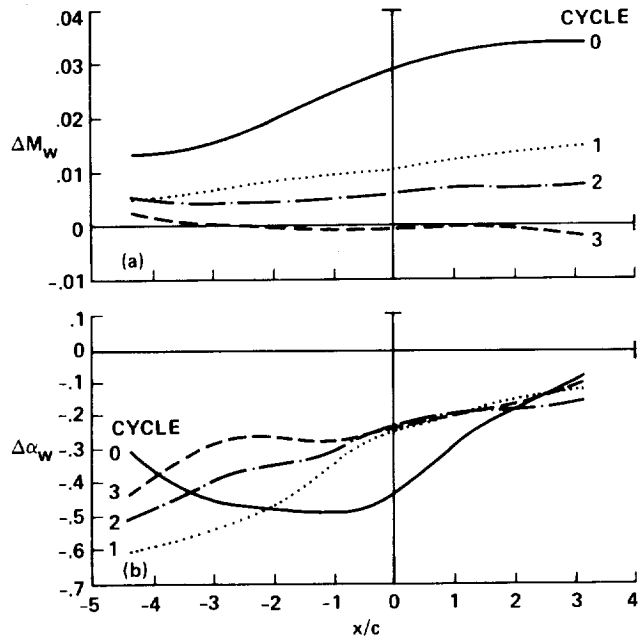

Figure 25.– Effect of wall adjustments on wall-induced velocities along test-section centerline: z/c = 0, M = 0.70, $\alpha = 2°$. (a) Wall-induced Mach number increment; (b) wall-induced flow angle.

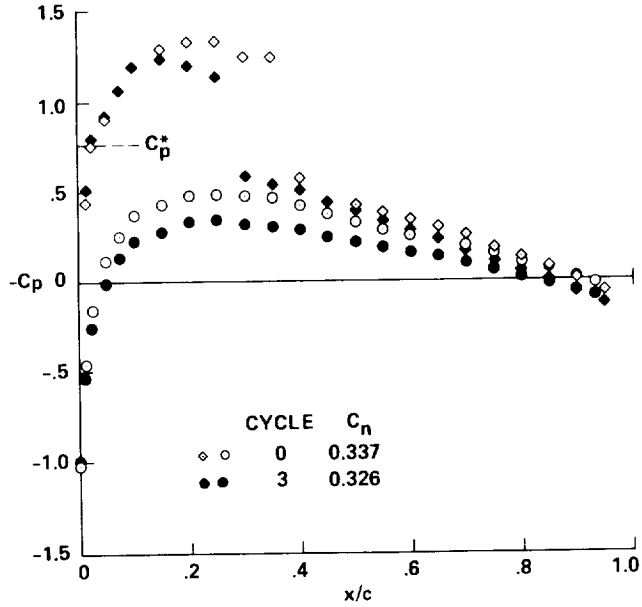

Figure 26.– Effect of wall adjustments on model pressure distribution: M = 0.70, $\alpha = 2°$.

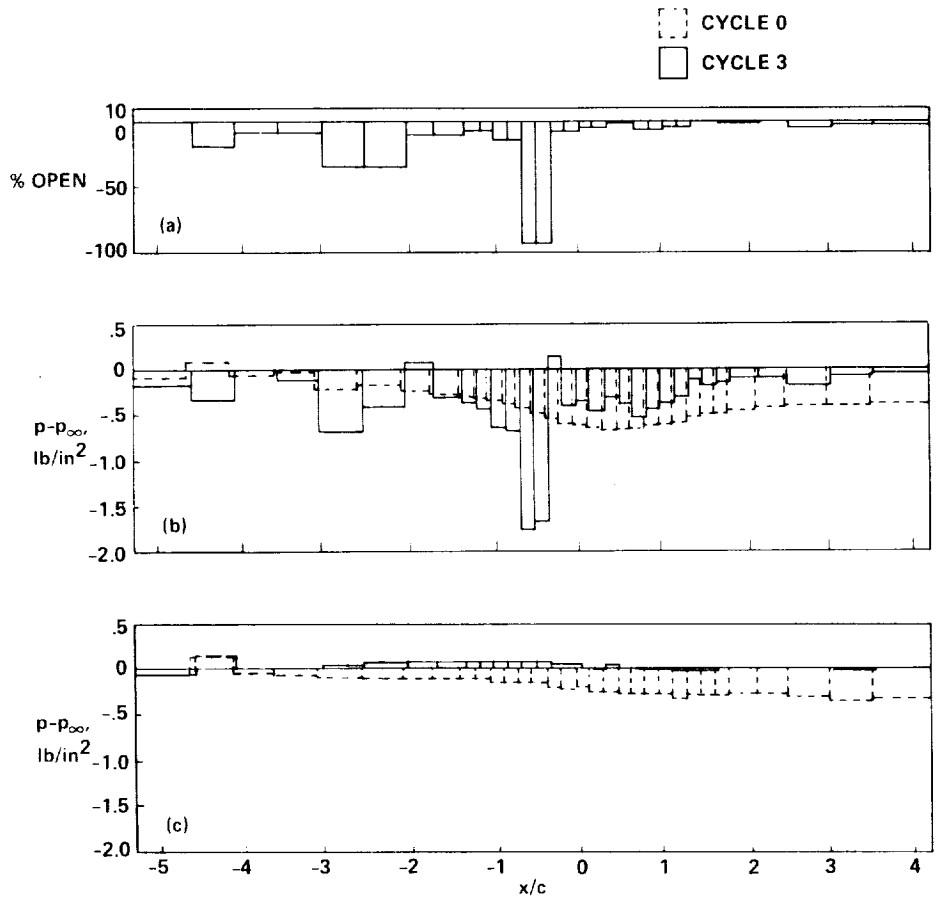

Figure 27.– Comparisons of initial and final slide-valve positions and plenum compartment pressures: M = 0.70, $\alpha = 2°$. (a) Slide-valve positions, top; (b) plenum pressures, top; (c) plenum pressures, bottom.

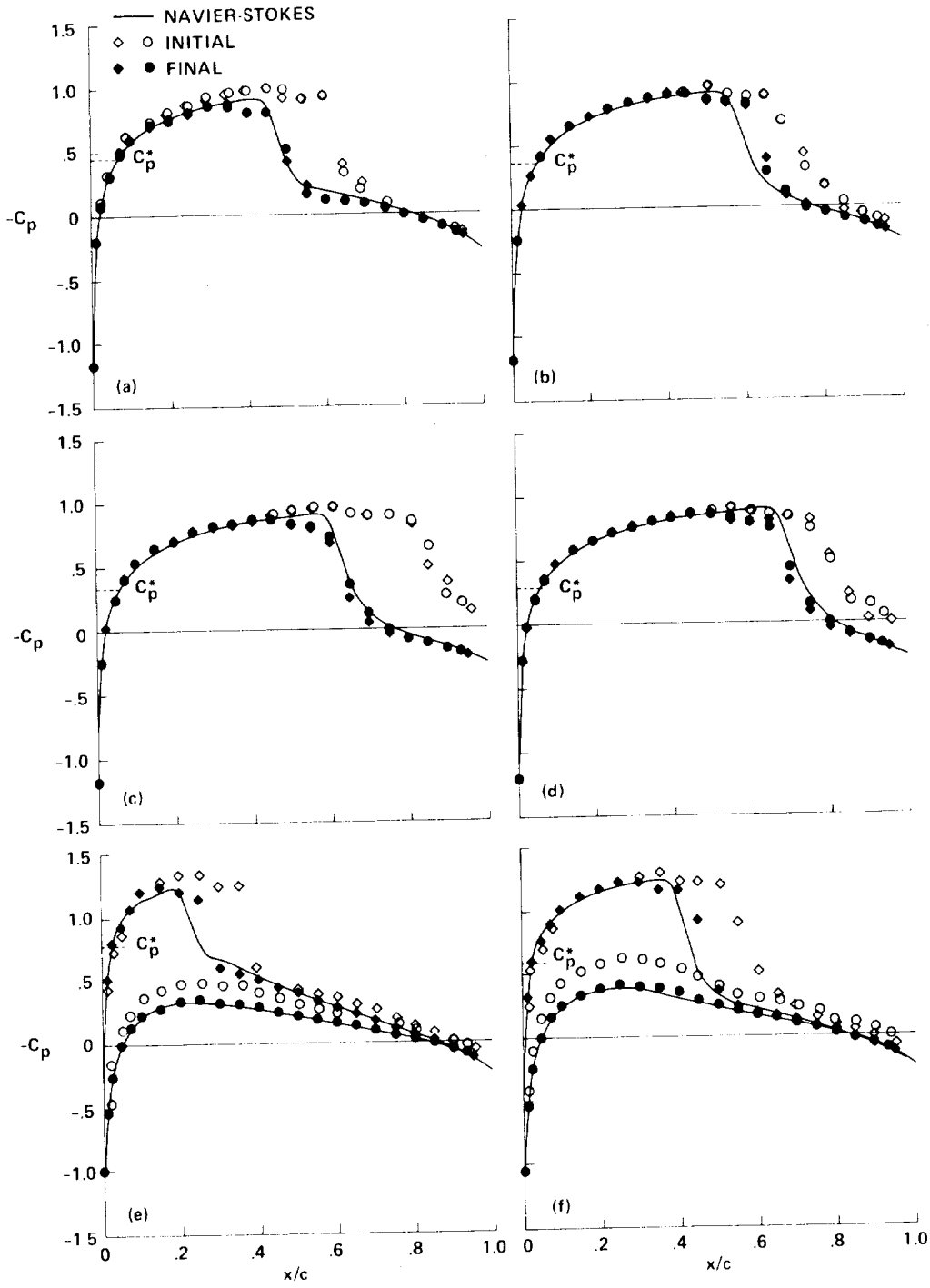

Figure 28.– Comparison of initial and final model pressure distributions with free-air Navier-Stokes solution. (a) $M = 0.80$, $\alpha = 0°$; (b) $M = 0.825$, $\alpha = 0°$; (c) $M = 0.835$, $\alpha = 0°$; (d) $M = 0.850$, $\alpha = 0°$; (e) $M = 0.70$, $\alpha = 2°$; (f) $M = 0.75$, $\alpha = 2°$.

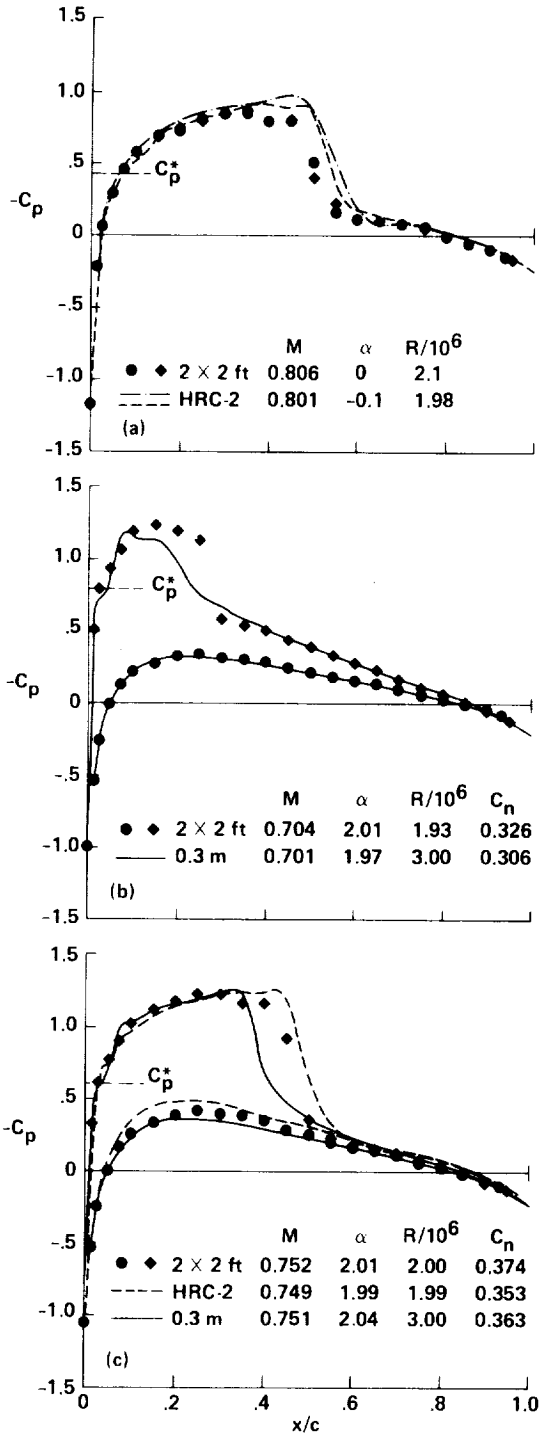

Figure 29.– Comparison of final model pressure distributions with data from Langley 0.3 M and Ames HRC-2 wind tunnels.

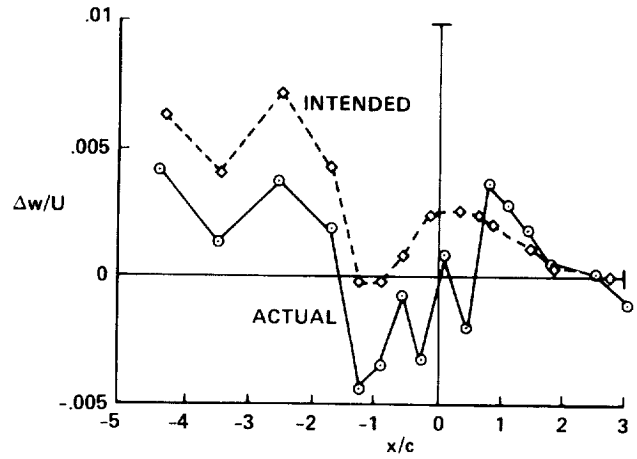

Figure 30.– Comparison of actual and predicted vertical velocity changes at measurement level resulting from one cycle of wall adjustments: M = 0.70, $\alpha = 2°$.

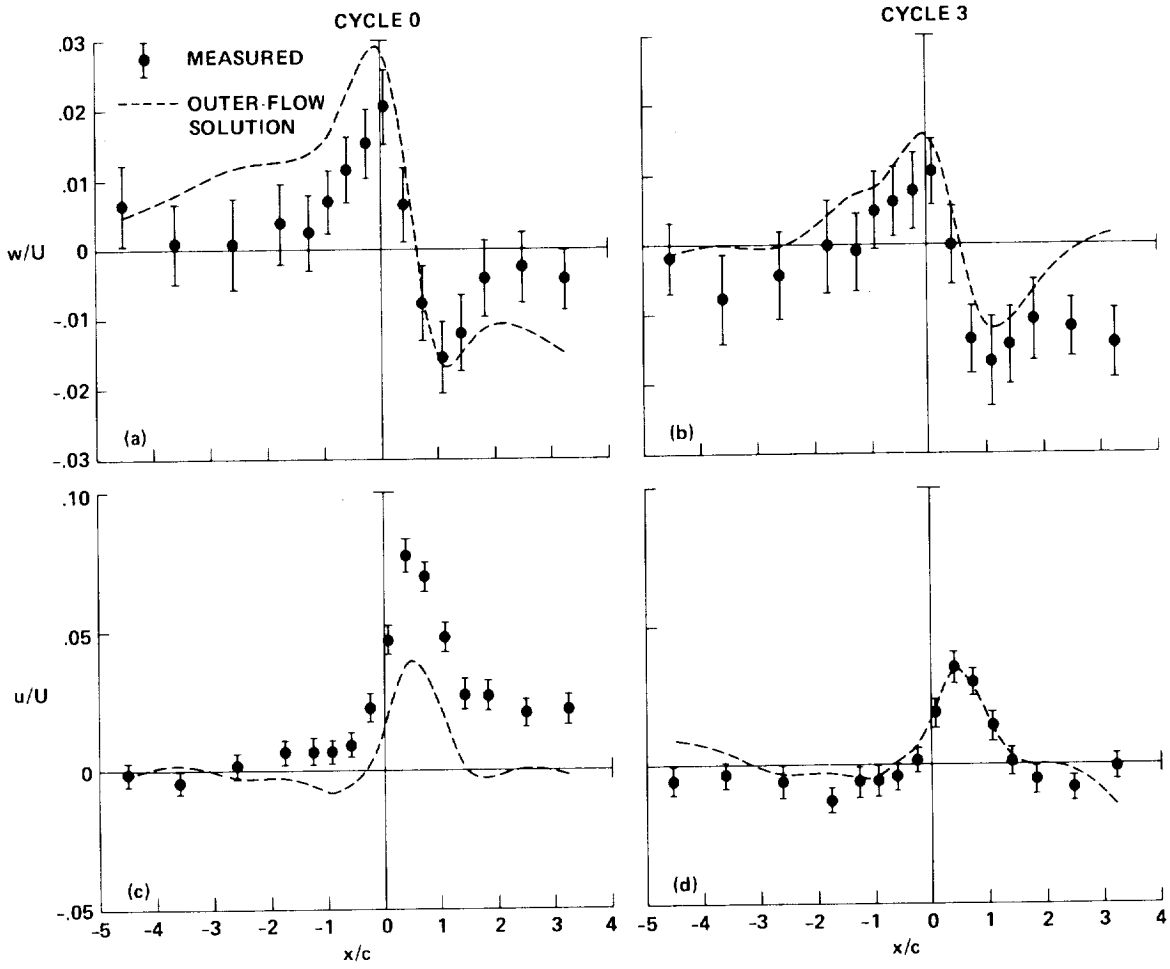

Figure 31.– Comparisons of measured velocity distributions with outer-flow solutions: z/c = 1.5, M = 0.80, $\alpha = 0°$. (a) Vertical velocity, cycle 0; (b) vertical velocity, cycle 3; (c) axial velocity, cycle 0; (d) axial velocity, cycle 3.

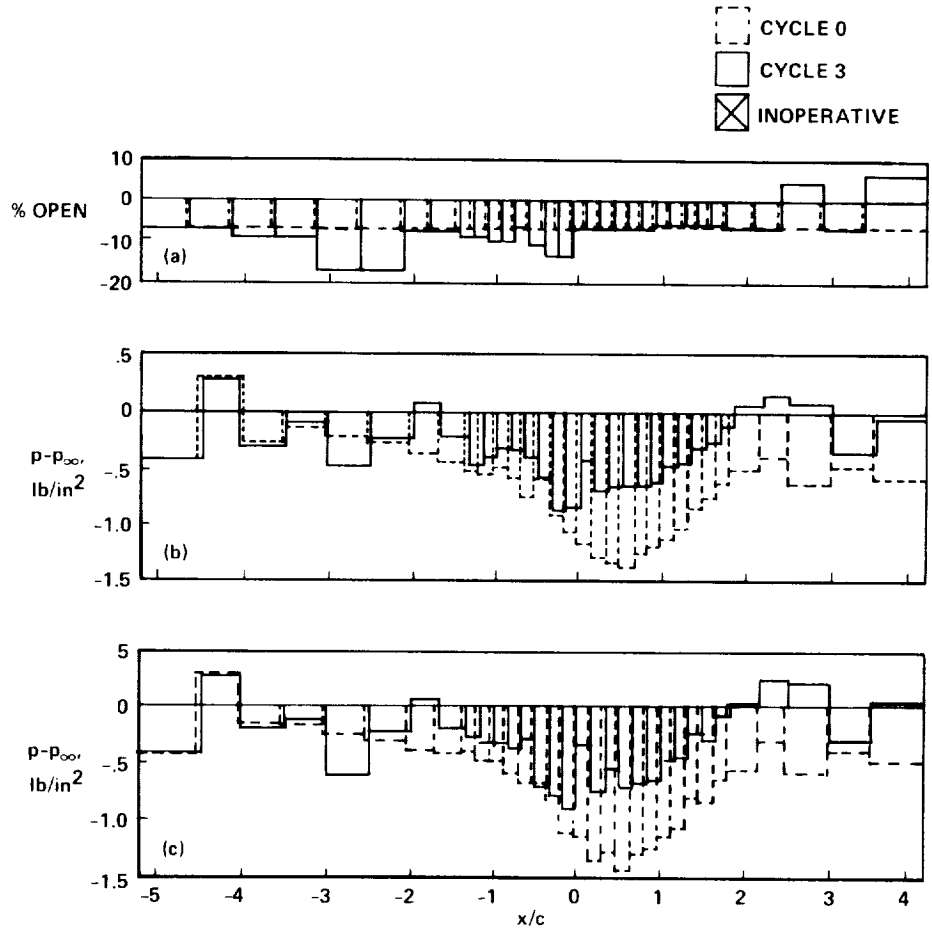

Figure 32.– Comparisons of initial and final slide-valve positions and plenum compartment pressures: M = 0.80, $\alpha = 0°$. (a) Slide-valve positions, top and bottom; (b) plenum pressures, top; (c) plenum pressures, bottom.

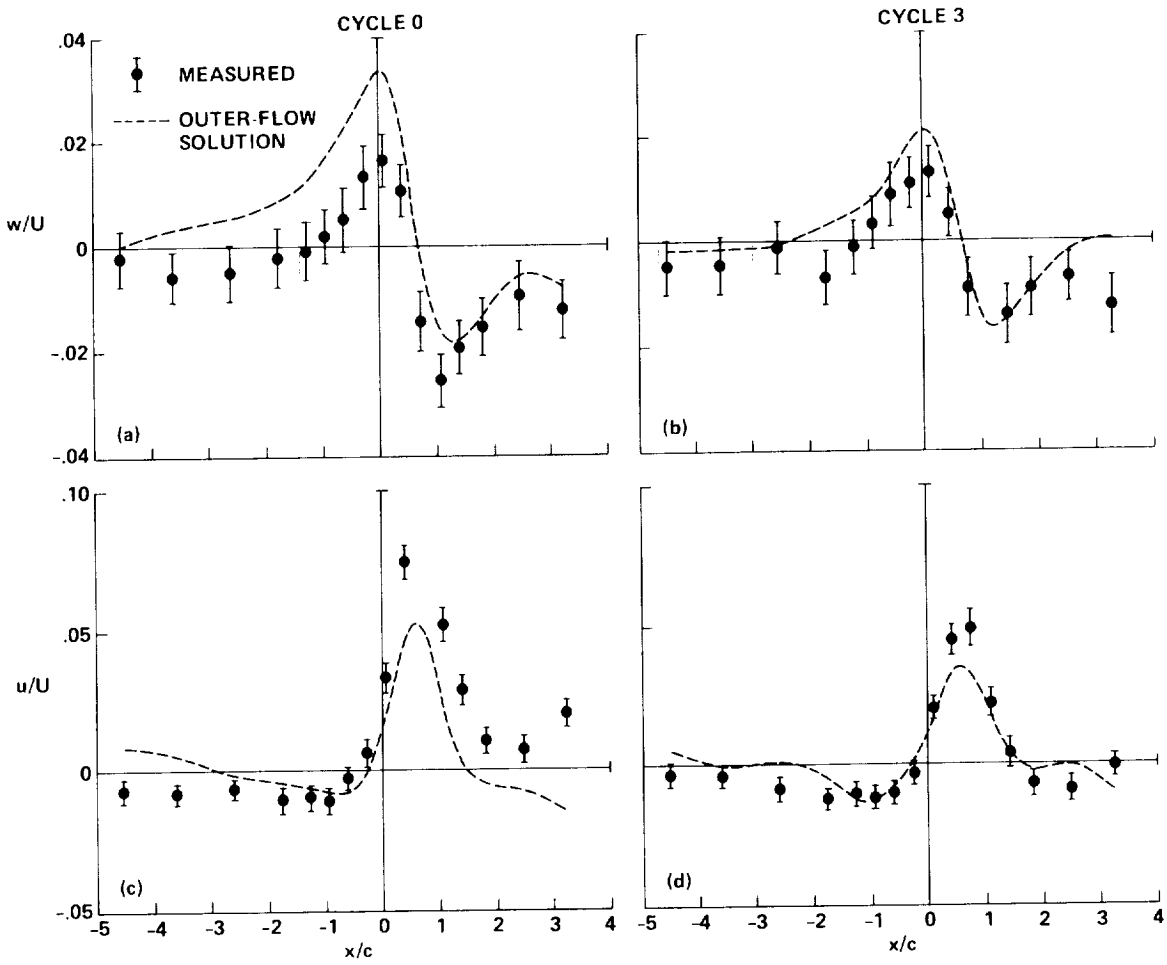

Figure 33.– Comparisons of measured velocity distributions with outer-flow solutions: z/c = 1.5, M = 0.825, $\alpha = 0°$. (a) Vertical velocity, cycle 0; (b) vertical velocity, cycle 3; (c) axial velocity, cycle 0; (d) axial velocity, cycle 3.

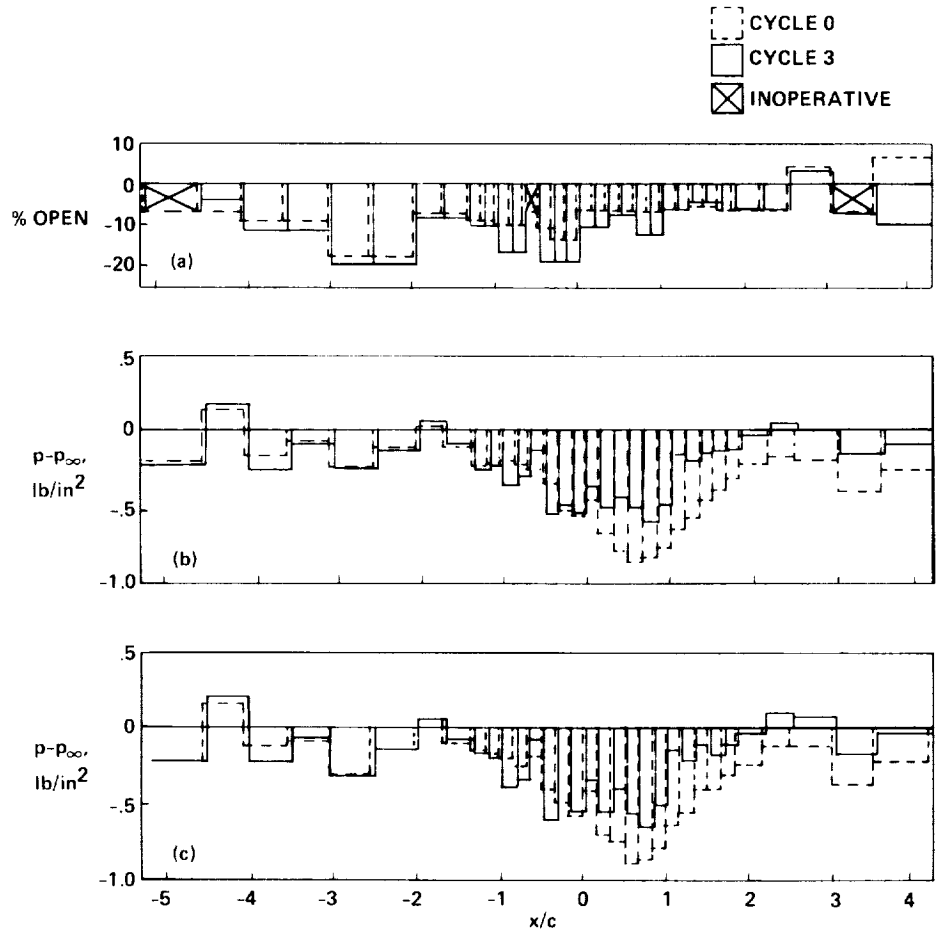

Figure 34.– Comparisons of initial and final slide-valve positions and plenum compartment pressures: M = 0.825, $\alpha = 0°$. (a) Slide-valve positions, top and bottom; (b) plenum pressures, top; (c) plenum pressures, bottom.

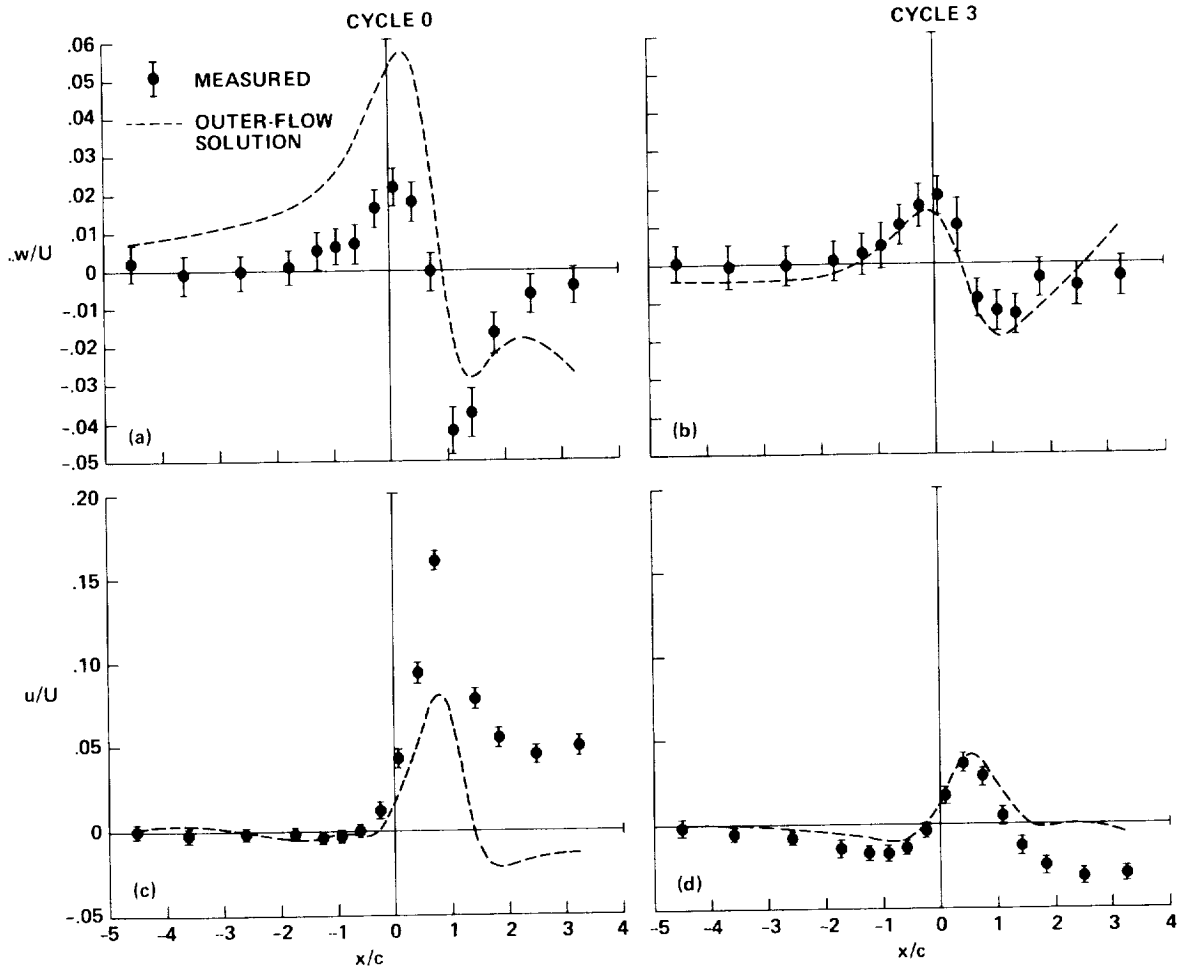

Figure 35.– Comparisons of measured velocity distributions with outer-flow solutions: z/c = 1.5, M = 0.835, $\alpha = 0°$. (a) Vertical velocity, cycle 0; (b) vertical velocity, cycle 3; (c) axial velocity, cycle 0; (d) axial velocity, cycle 3.

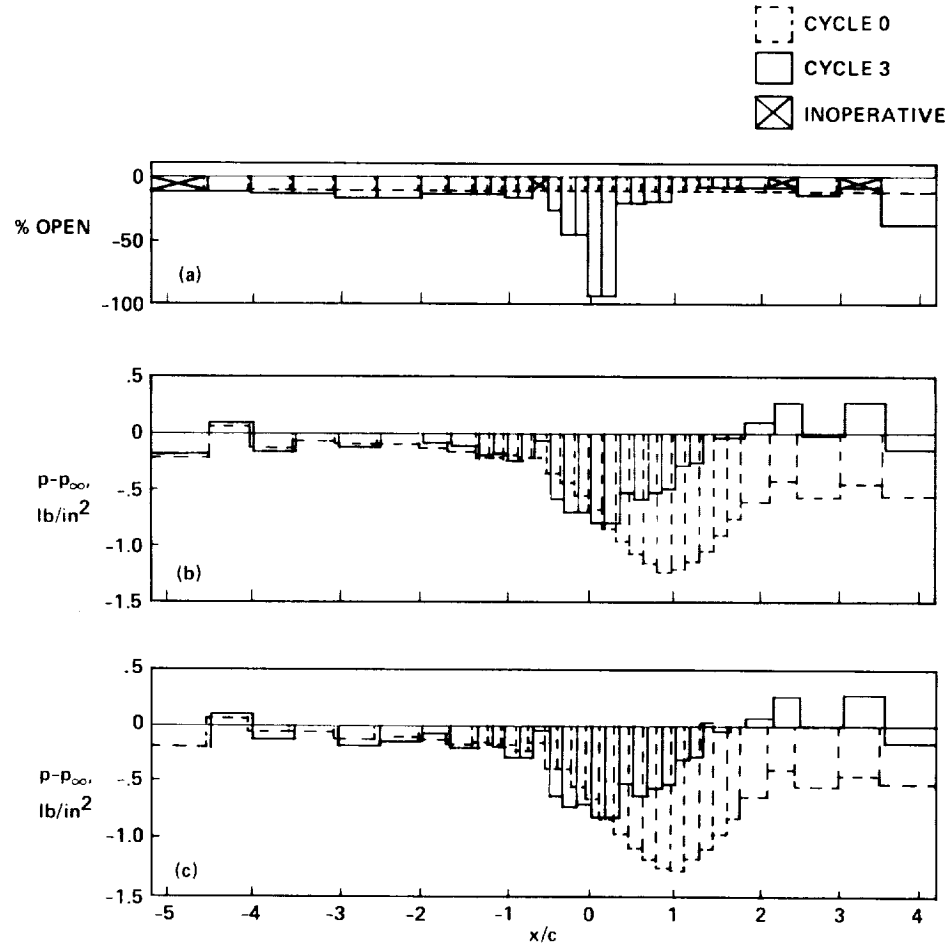

Figure 36.– Comparisons of initial and final slide-valve positions with plenum compartment pressures: M = 0.835, $\alpha = 0°$. (a) Slide-valve positions, top and bottom; (b) plenum pressures, top; (c) plenum pressures, bottom.

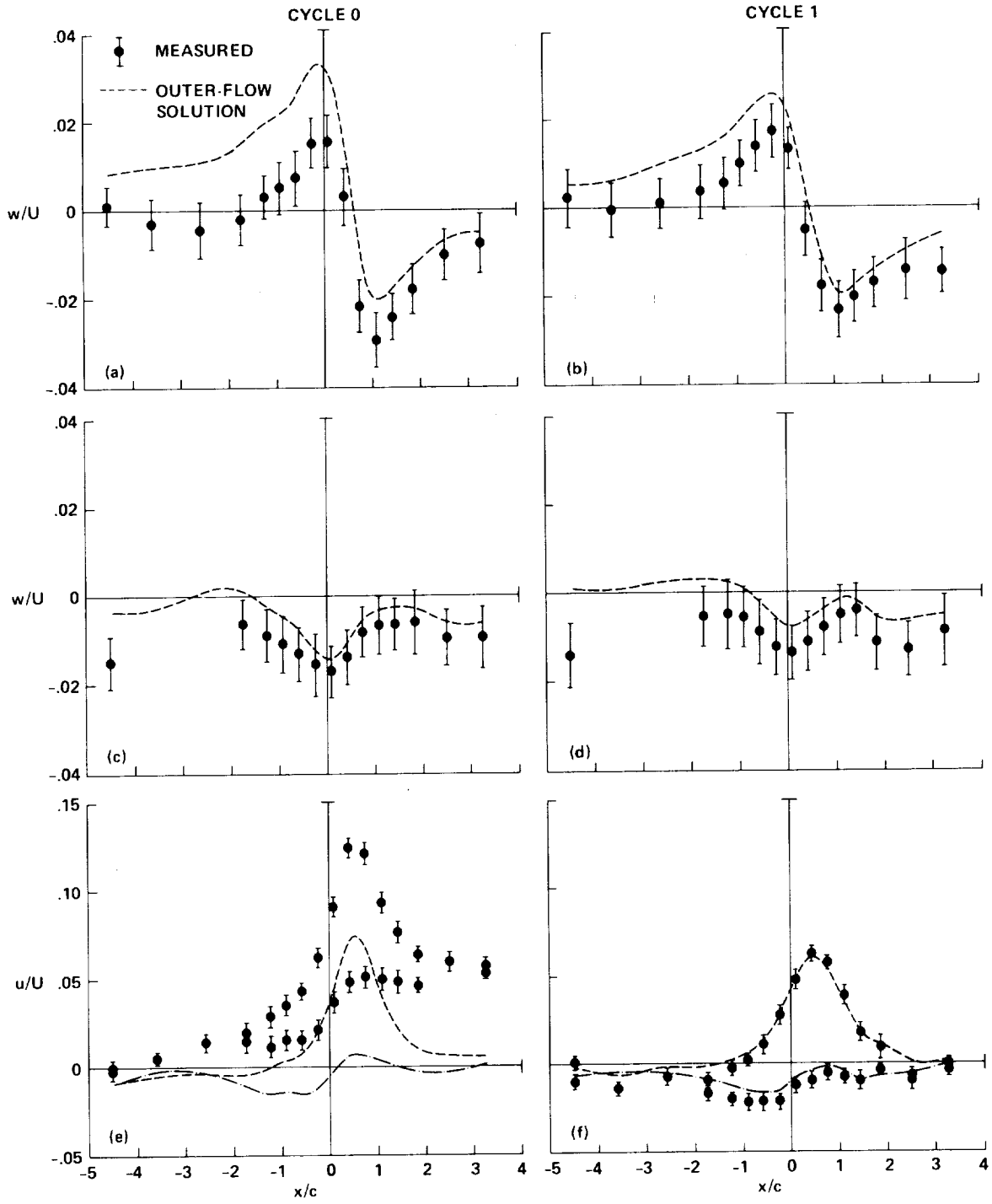

Figure 37.– Comparisons of measured velocity distributions with outer-flow solutions: z/c = 1.5, M = 0.75, $\alpha = 2°$. (a) Vertical velocity, z/c = 1.5, cycle 0; (b) vertical velocity, z/c = 1.5, cycle 1; (c) vertical velocity, z/c = –1.5, cycle 0; (d) vertical velocity, z/c = –1.5, cycle 1; (e) axial velocity, z/c = ±1.5, cycle 0; (f) axial velocity, z/c = ±1.5, cycle 1.

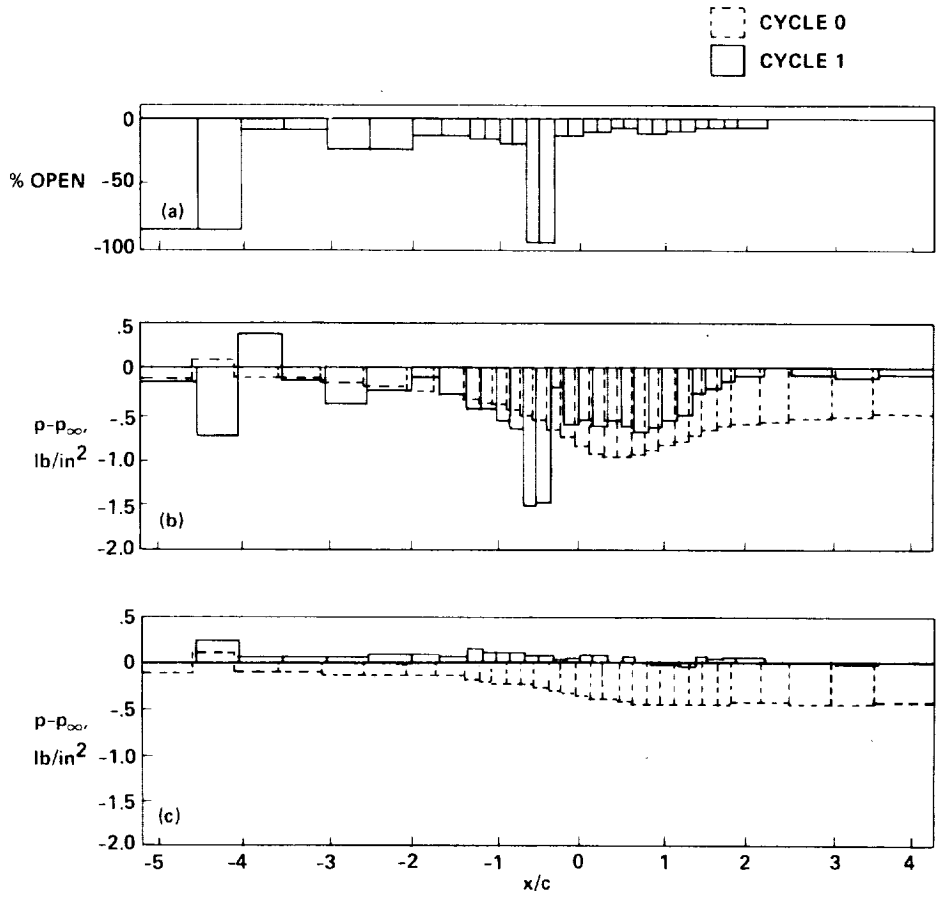

Figure 38.– Comparisons of initial and final slide-valve positions with plenum compartment pressures: $M = 0.75$, $\alpha = 2°$. (a) Slide-valve positions, top; (b) plenum pressures, top; (c) plenum pressures, bottom.

NASA
National Aeronautics and Space Administration

Report Documentation Page

1. Report No.	2. Government Accession No.	3. Recipient's Catalog No.
NASA TM-102207		

4. Title and Subtitle	5. Report Date
A Two-Dimensional Adaptive-Wall Test Section with Ventilated Walls in the Ames 2- by 2-Foot Transonic Wind Tunnel	August 1989
	6. Performing Organization Code

7. Author(s)	8. Performing Organization Report No.
Edward T. Schairer, George Lee, and T. Kevin McDevitt (Complere, Inc., Palo Alto, CA)	A-89195
	10. Work Unit No. 505-61-01

9. Performing Organization Name and Address	11. Contract or Grant No.
Ames Research Center Moffett Field, CA 94035	
	13. Type of Report and Period Covered Technical Memorandum

12. Sponsoring Agency Name and Address	14. Sponsoring Agency Code
National Aeronautics and Space Administration Washington, DC 20546-0001	

15. Supplementary Notes

Point of Contact: Edward T. Schairer, Ames Research Center, MS 260-1, Moffett Field, CA 94035
(415) 694-3656 or FTS 464-3656

16. Abstract

The first tests conducted in the adaptive-wall test section of the Ames Research Center's 2- by 2-Foot Transonic Wind Tunnel are described. A procedure was demonstrated for reducing wall interference in transonic flow past a two-dimensional airfoil by actively controlling flow through the slotted walls of the test section. Flow through the walls was controlled by adjusting pressures in compartments of plenums above and below the test section. Wall interference was assessed by measuring (with a laser velocimeter) velocity distributions along a contour surrounding the model, and then checking those measurements for their compatibility with free-air far-field boundary conditions. Plenum pressures for minimum wall interference were determined from empirical influence coefficients.

An NACA 0012 airfoil was tested at angles of attack of 0° and 2°, and at Mach numbers between 0.70 and 0.85. In all cases the wall-setting procedure greatly reduced wall interference. Wall interference, however, was never completely eliminated, primarily because the effect of plenum pressure changes on the velocities along the contour could not be accurately predicted.

17. Key Words (Suggested by Author(s))	18. Distribution Statement
Wall interference Wind tunnel Adaptive walls NACA 0012 airfoil	Unclassified-Unlimited Subject Category - 09

19. Security Classif. (of this report)	20. Security Classif. (of this page)	21. No. of Pages	22. Price
Unclassified	Unclassified	59	A04